https://doi.org/10.5194/essd-2026-521
Preprint. Discussion started: 14 July 2026

Open Access Earth System Science Data Discussions

Ise Bay Reanalysis (IBRA): An Ecological Hydrodynamic Dataset Based on EcoPARI

Yoshitaka Matsuzaki[1], Hayato Mizuguchi[1,2], Tetsunori Inoue[3,4,5,6]

[1]Marine Pollution Management Group, Port and Airport Research Institute, 3-1-1 Nagase, Yokosuka, Kanagawa, 239-0826, Japan
[2]ECOH Corporation Co., Ltd., 2-6-4 KitaUeno, Taito-ku, Tokyo, 110-0014, Japan
[3]Senior Director for Research Affairs, Port and Airport Research Institute, 3-1-1 Nagase, Yokosuka, Kanagawa, 239-0826, Japan
[4]Estuary Research Center, Shimane University, 1060 Nishikawatsu-cho, Matsue, Shimane 690-8504, Japan
[5]Department of Transdisciplinary Science and Engineering, Tokyo Institute of Technology, 4259 Nagatsuta-cho, Midori-ku, Yokohama, Kanagawa 226-8503, Japan
[6]College of Life and Environmental Sciences, Wenzhou University, Wenzhou, Zhejiang, 325035, China

Correspondence to: Yoshitaka Matsuzaki (matsuzaki-y@p.mpat.go.jp)

Abstract. Reanalysis datasets based on coupled ocean circulation and ecosystem models are essential tools for understanding coastal environmental variability and supporting water quality management. However, the development of such datasets for highly enclosed coastal systems remains limited, particularly those incorporating subsurface biogeochemical observations, such as dissolved oxygen (DO). This study presents the Ise Bay Reanalysis (IBRA), a 12-year (2011–2022), high-resolution reanalysis dataset of hydrodynamic and biogeochemical variables for Ise Bay, Japan. The dataset was generated using the Ecological hydrodynamic simulation system of the Port and Airport Research Institute (EcoPARI)-simulator, coupled with an ensemble Kalman filter data assimilation system that assimilates in situ observations of water temperature, salinity, and bottom-layer DO at 6 h intervals. The resulting dataset has an hourly temporal resolution and resolves the full water column. IBRA has three key distinguishing features: first, unlike many previous reanalysis datasets that rely primarily on satellite observations, IBRA assimilates continuous in situ measurements throughout the water column, including high-frequency DO observations, allowing improved representation of subsurface dynamics; second, the 6-hour assimilation cycle enables the dataset to resolve short-term variability driven by tidal processes, which are a dominant control on coastal transport and mixing; third, spatially coherent corrections are applied over the entire bay using an ensemble Kalman filter, ensuring spatial consistency of both physical and biogeochemical fields while avoiding artificial discontinuities often associated with simpler assimilation approaches. Its quality was evaluated using statistical metrics and detailed comparisons with in situ observations. Data assimilation improved the overall agreement with observations across multiple stations and depths, particularly for bottom-layer DO. The dataset successfully reproduced seasonal variability, vertical stratification, and the formation and persistence of hypoxic conditions in the inner bay, while also capturing well-oxygenated conditions near the bay mouth. Furthermore, the spatial distributions of temperature, salinity, and DO were realistically represented, including the intrusion of offshore water masses and associated horizontal gradients. The IBRA dataset thus provides a dynamically consistent and

https://doi.org/10.5194/essd-2026-521
Preprint. Discussion started: 14 July 2026

comprehensive description of both physical and biogeochemical variability in a highly enclosed coastal system. It is expected to serve as a valuable resource for studies of coastal hypoxia, water quality assessment, and environmental management.

1 Introduction

Model systems that combine realistic representations of ocean circulation with biogeochemical or ecosystem models are valuable tools for analysis and prediction (Fennel et al., 2019). Accordingly, a demand has grown for reanalysis datasets based on coupled hydrodynamic–ecosystem models, and several advanced studies have been conducted in this area. For example, Ford and Barciela (2017) produced global marine biogeochemical reanalysis for the period 1997–2012 by assimilating ocean-color-derived chlorophyll data into a physical–biogeochemical ocean model. Ciavatta et al. (2018) conducted a reanalysis of the northeast Atlantic, including the northwest European continental shelf, covering 1998–2003, characterized by the assimilation of phytoplankton functional types derived from ocean color observations into an ecosystem model. Von Schuckmann et al. (2018) used multiyear biogeochemical reanalysis driven by physical reanalysis fields and assimilated satellite chlorophyll observations to evaluate biogeochemical variability and long-term trends, with target periods typically spanning the most recent 10–15 years. Cossarini et al. (2021) developed a reanalysis dataset for the Mediterranean Sea covering 1999–2019, at a horizontal resolution of 1/24°. Global biogeochemical reanalysis datasets have also been published (Chamberlain et al., 2021), providing long-term, basin-scale reconstructions constrained primarily by satellite observations and limited in situ data.

These previous studies have relied primarily on satellite-derived observations, which are largely limited to the sea surface; consequently, their capacity to resolve subsurface biogeochemical variability remains limited. In highly enclosed coastal systems, complex interactions among tides, stratification, and biogeochemical processes introduce stronger spatiotemporal variability than is typically observed in the open ocean. Regional coastal reanalysis efforts have also been made using data-assimilative models. For example, Wilkin et al. (2022) produced a data-assimilative circulation reanalysis for the U.S. Mid-Atlantic Bight and the Gulf of Maine employing the Regional Ocean Modeling System with four-dimensional variational data assimilation, incorporating satellite, coastal radar, and in situ observations. However, these studies have primarily focused on physical circulation, and applications incorporating fully coupled ecosystem dynamics remain limited. Therefore, the assimilation of subsurface observational data is crucial in highly enclosed coastal systems. These factors render reanalysis in such environments more challenging. To the best of our knowledge, reanalysis datasets that directly assimilate oxygen observations remain rare. In Japan, the Ministry of the Environment has been gradually implementing environmental standards for bottom-layer dissolved oxygen (DO) levels in enclosed water bodies and lakes. Therefore, understanding the spatiotemporal distribution of bottom-layer DO is expected to become increasingly important, both scientifically and politically.

In this study, we developed the Ise Bay Reanalysis (IBRA), a 12-year (2011–2022) reanalysis dataset of hydrodynamics and aquatic ecosystem variables for Ise Bay, Japan, using the numerical model (Tanaka and Suzuki, 2010; Tanaka et al., 2011;

https://doi.org/10.5194/essd-2026-521
Preprint. Discussion started: 14 July 2026

Matsuzaki et al., 2024) and a data assimilation system (Matsuzaki and Inoue, 2022) of the Ecological hydrodynamic simulation system of the Port and Airport Research Institute (EcoPARI). The dataset presented here extends a hydrodynamic reanalysis dataset (Matsuzaki et al., 2025a) by coupling an ecosystem model and assimilating bottom-layer DO observations. IBRA was developed as part of a research project funded by the Environmental Research and Technology Development Fund of the Environmental Restoration and Conservation Agency (JPMEERF20221R01), Ministry of the Environment, Japan. The development of IBRA was motivated by the designation of water quality classifications based on bottom-layer DO concentration in Ise Bay and aims to provide scientific information to support assessments of compliance with these environmental quality standards. Its distinguishing features are elucidated in the subsequent parts of this section.

The present study assimilates continuous in situ observations of key biogeochemical parameters (water temperature, salinity, and DO) collected by fixed monitoring stations spanning the entire water column from the sea surface to the seabed. This ensures high temporal-resolution data assimilation and greater reliability, which is unique to this study. With the chosen data volume, our study addresses the limitations of satellite-derived sea surface data identified in previous studies aimed at developing hydrodynamic–ecosystem reanalysis datasets.

Second, data assimilation was performed at 6 h intervals, enabling the dataset to account for the short-term variability associated with tidal currents (Mizuguchi et al., 2025), which are a dominant driver of physical and biogeochemical transport in coastal waters. The output dataset was generated from free-running simulations initialized from each analysis state and integrated for 6 h, yielding hourly-resolution data.

Third, background states were corrected over the entire bay through data assimilation using spatial correlations derived from an ensemble Kalman filter, thereby ensuring the spatial consistency of the analyzed fields (Matsuzaki and Inoue, 2022). In other words, the dataset was designed to avoid the spatial discontinuities in physical and biogeochemical variables that often arise from simple nudging approaches or non-physical localization techniques.

This study describes the development of IBRA and evaluates its suitability through quantitative accuracy metrics and qualitative comparisons with observed spatial distributions. The remainder of this paper is organized as follows: Section 2 describes the hydrodynamic–ecosystem model, data assimilation system, and assimilated observations. Section 3 presents the quality assessment of the reanalysis dataset. Section 4 presents the discussion of the three features of this reanalysis dataset. Section 5 describes the available outputs, data access methods, and file structures. Section 6 presents the conclusions and potential applications of IBRA and provides concluding remarks.

2 Materials and methods

2.1 Simulation model and setup

The simulation model and its setup were adapted from previously described configurations (Matsuzaki and Inoue, 2022; Matsuzaki and Kubota, 2024; Matsuzaki et al., 2025b). The model domain covers Ise Bay (Figure **1**), with an area of 2,342

https://doi.org/10.5194/essd-2026-521
Preprint. Discussion started: 14 July 2026

km^2, a volume of 3.94×10^{10} m^3, an average depth of 17 m, and a maximum depth of 100 m (https://www.cbr.mlit.go.jp/kikaku/sai_ise/pdf/koudou_01.pdf, accessed on March 25, 2026). The bay is located in the south-central region of Honshu Island, Japan, and extends 70 km in both the longitudinal and latitudinal directions. The lateral boundary is connected to the Pacific Ocean, and the annual river discharge is 2.0×10^{10} m^3, which is approximately half of the volume of Ise Bay. Ise Bay receives inputs from 10 Class A rivers (Table S1 in the Supplementary Materials) and 76 smaller rivers. The Kiso, Ibi, and Nagara rivers, which contribute the greatest discharges, flow from the rear of the bay (Figure **1**). Seasonal wind patterns include northwesterly winds from autumn to spring, whereas sea and land breezes predominate during summer, blowing from the southeast during the day and from the northwest at night (Sekine et al., 2002).

Simulations were conducted using EcoPARI-Simulator, an ecological hydrodynamics simulation system of the Port and Airport Research Institute of Japan (Matsuzaki et al., 2024; Tanaka and Suzuki, 2010; Tanaka et al., 2011). EcoPARI-Simulator uses a Cartesian coordinate system to simulate coastal and estuarine current dynamics, with a horizontal resolution of 800 m in both the x- and y-directions. The horizontal resolution (800 m) was determined through a trade-off between the accurate representation of bathymetry at the mouth of Ise Bay and computational cost. The coordinate system was rotated 45° clockwise, and EcoPARI-Simulator used a z-coordinate system. The vertical grid comprised 38 layers, with spacings of 0.5 m from the surface to 4 m, 1 m from 4 to 11 m, 2 m from 11 to 41 m, 9 m from 41 to 50 m, 20 m from 50 to 70 m, and 30 m from 70 to 100 m. Bathymetric data were obtained from the Japan Coast Guard. A subgrid-scale model (Smagorinsky, 1963) was used as the horizontal turbulence model, and the model proposed by Munk and Anderson (1948) was used as the vertical turbulence model. The Sommerfeld radiation condition was applied as the transmission condition at the lateral boundary (Orlanski, 1976). The governing equations for water temperature, salinity, and DO considered in this study were scalar transport equations, the details of which can be found in previous studies (Hafeez et al., 2021; Matsuzaki et al., 2025b; Tanaka and Suzuki, 2010; Tanaka et al., 2011).

https://doi.org/10.5194/essd-2026-521
Preprint. Discussion started: 14 July 2026

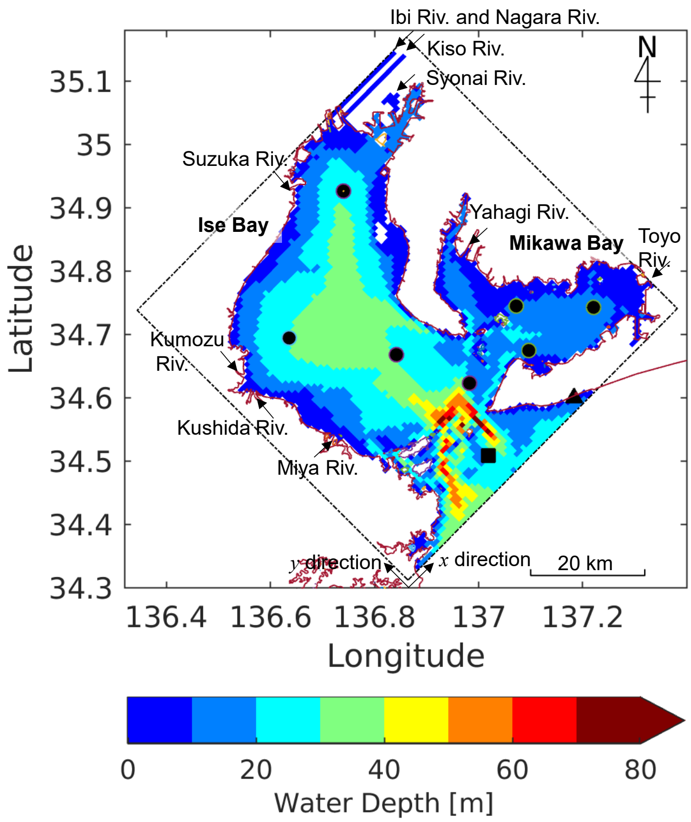

Figure 1: Location map of Ise Bay, Japan. The dashed-dotted line indicates the computational domain for the numerical model and data assimilation. The square denotes the observation point utilized to prescribe the lateral boundary conditions for water temperature and salinity. The triangle indicates the observation point used as a lateral boundary condition for tide levels. Water depth is represented by color. Arrows indicate the inflow positions and directions of the 10 Class A rivers. The northeast and northwest axes depict the computational grid in the x and y directions, with a grid size of 85 × 85 and a grid spacing of 800 m.

2.2 Boundary condition settings

Three types of boundary conditions were prescribed: lateral, atmospheric, and river discharge. The lateral boundary conditions for seawater temperature and salinity were derived from observational data collected near the open boundary (black square in Figure **1**). In addition, the observed water elevations at a station near the lateral boundary (black triangle in Figure **1**) were imposed as boundary conditions. Atmospheric forcing data were obtained from two datasets: (i) the Japan Meteorological Agency's Grid Point Value of the Meso-scale Model (GPV-MSM) for the simulation period from January 1, 2011, to December 31, 2016; (ii) the Japan Meteorological Agency's Grid Point Value of the Local Forecast Model (GPV-LFM; https://www.jma.go.jp/jma/kishou/know/whitep/1-3-6.html, accessed March 17, 2026) for the simulation period from January 1, 2017, to December 31, 2022. These two datasets were used because the more recent GPV-LFM has been available since January 2016, whereas before that, only the GPV-MSM dataset was available. River discharge boundary conditions were

https://doi.org/10.5194/essd-2026-521
Preprint. Discussion started: 14 July 2026

specified using observational data. Further details of the boundary condition settings are provided in the Supplementary Material.

2.3 Assimilation model

The simulation model and its setup were adapted from previously described configurations (Matsuzaki and Inoue, 2022). The Ensemble Kalman Filter (EnKF) model for the Ise Bay Simulator was coded as described by Evensen (2003). The basic analysis steps of the Kalman filter and EnKF have been explained subsequently in detail. The analysis value $\boldsymbol{x}^{a}$ (data assimilation results) at a certain time t is obtained by the optimal weighted average of the background value $\boldsymbol{x}^{f}$ (forecast/simulation results) and the observed value $\boldsymbol{y}$, as shown in Equation (1):

$$\boldsymbol{x}_t^a = \boldsymbol{x}_t^f + \boldsymbol{K}_t\left(\boldsymbol{y}_t - \boldsymbol{H}_t\boldsymbol{x}_t^f\right) \quad (1)$$

where $\boldsymbol{x}$ represents a state vector whose elements are physical and ecosystem quantities, such as water temperature, salinity, current velocity, phytoplankton concentration, and DO concentration in each mesh of the numerical model; $\boldsymbol{y}$ is an observation vector with the observed values of water temperature, salinity, phytoplankton concentration, and DO as elements; $\boldsymbol{H}$ is an observation matrix and an operator that extracts the physical and ecosystem quantities of the mesh corresponding to the observation point from the results (state vector) of the numerical model; $\boldsymbol{K}$ is a weight matrix (Kalman gain) that determines the extent to which the observed values are assimilated. $\boldsymbol{K}$ is calculated as follows:

$$\boldsymbol{K}_t = \boldsymbol{P}_t^f\boldsymbol{H}_t^T\left(\boldsymbol{R}_t + \boldsymbol{H}_t\boldsymbol{P}_t^f\boldsymbol{H}_t^T\right)^{-1} \quad (2)$$

where $\boldsymbol{P}$ is the background error covariance matrix, and $\boldsymbol{R}$ is the observation error covariance matrix; the superscript T indicates the transpose. Equation (2) shows that the assimilation rate of the observed values is determined by the relationship between $\boldsymbol{P}$ and $\boldsymbol{R}$, and that the spatial correction by the observed values is determined by $\boldsymbol{P}$. As mentioned in the Introduction, the main purpose of this study is to calculate appropriate ensembles for regional coastal estuary modeling, which depends on the background error covariance matrix $\boldsymbol{P}$. The data assimilation flow in the EnKF is as follows:

a) Ensemble members were calculated using the EcoPARI-Simulator numerical model. In this study, ensemble members were calculated under different boundary conditions, as described in Sect. 2.4. The number of ensembles was expressed as L.

b) The background error covariance matrix is estimated from ensembles.

$$\overline{\boldsymbol{P}}_t^f = \frac{1}{L-1}\sum_{l=1}^{L}\left(\boldsymbol{x}_t^{f(l)} - \overline{\boldsymbol{x}}_t^f\right)\left(\boldsymbol{x}_t^{f(l)} - \overline{\boldsymbol{x}}_t^f\right)^T \quad (3)$$

$$\overline{\boldsymbol{x}}_t^f = \frac{1}{L}\sum_{l=1}^{L}\boldsymbol{x}_t^{f(l)} \quad (4)$$

Here, the ensemble mean and overbars denote covariance matrix.

c) The observation error covariance matrix is estimated from ensembles.

$$\overline{\boldsymbol{R}}_t = \frac{1}{L-1}\sum_{l=1}^{L}\left(\boldsymbol{r}_t^{(l)} - \overline{\boldsymbol{r}}_t\right)\left(\boldsymbol{r}_t^{(l)} - \overline{\boldsymbol{r}}_t\right)^T \quad (5)$$

https://doi.org/10.5194/essd-2026-521
Preprint. Discussion started: 14 July 2026

$$\bar{\boldsymbol{r}}_t = \frac{1}{L}\sum_{l=1}^{L} \boldsymbol{r}_t^{(l)} \tag{6}$$

where $\boldsymbol{r}$ is the observation error, comprising the measurement error attributable to the characteristics of the observation equipment and the measurement environment, and the expression error arising from phenomena that the numerical model cannot express.

d) The Kalman gain is estimated as follows:

$$\overline{\boldsymbol{K}}_t = \overline{\boldsymbol{P}}_t^f \boldsymbol{H}_t^T \left(\overline{\boldsymbol{R}}_t + \boldsymbol{H}_t \overline{\boldsymbol{P}}_t^f \boldsymbol{H}_t^T\right)^{-1} \tag{7}$$

e) The analysis values of ensemble members are calculated as follows:

$$\boldsymbol{x}_t^{a(l)} = \boldsymbol{x}_t^{f(l)} + \overline{\boldsymbol{K}}_t\left(\boldsymbol{y}_t + \boldsymbol{r}_t^{(l)} - \boldsymbol{H}_t \boldsymbol{x}_t^{f(l)}\right) \quad (l = 1, \dots, L) \tag{8}$$

The average $\overline{\boldsymbol{x}}_t^a$ of the analysis values for each ensemble member is the data assimilation result.

$$\overline{\boldsymbol{x}}_t^a = \frac{1}{L}\sum_{l=1}^{L} \boldsymbol{x}_t^{a(l)} \tag{9}$$

The settings for the ensemble simulation were the same as those described in Sect. 2.1, and a novel data assimilation method with a high-resolution horizontal grid size (800 m) was employed. EnKF was implemented using 32 members (L = 32). The ensemble number was selected as described in a previous study (Matsuzaki and Inoue, 2022). The observation data described below were assimilated once every 6 h at 00:00, 6:00, 12:00, and 18:00. The localization technique (Evensen, 2009; Gaspari and Cohn, 1999; Hamill et al., 2001) was not applied; thus, it was possible to correct the entire Ise Bay domain based on the background error covariance using a coupled physical and ecosystem model, rather than using non-physical techniques such as the distance function. The multiplicative inflation technique was not applied because it generates non-physical, non-ecosystem, and spurious error covariances (Sanikommu et al., 2020). Moreover, the correlation between observation errors was ignored; that is, the observation error covariance matrix was assumed to be diagonal. As explained in Sect. 2.4, perturbations were added to the boundary conditions and parameters to represent system error. When assimilation was performed near the lateral boundary and the three largest rivers (the Kiso, Ibi, and Nagara rivers) were included, the assimilation system became unstable. To stabilize data assimilation, variables on the two meshes adjacent to the lateral boundary and those near the mouths of the three rivers were excluded from the Kalman gain calculation and assimilation, thereby ensuring stable data assimilation performance.

2.4 Method of adding perturbations to boundary conditions and parameters

Generating a perturbation and determining its magnitude were based on Matsuzaki and Inoue (2022). Equations (10) and (11) were used to add perturbations to the boundary conditions:

$$\boldsymbol{F}_{mem} = \boldsymbol{F}_{base} + \boldsymbol{v} \tag{10}$$

$$\boldsymbol{F}_{mem} = (\boldsymbol{1} + \boldsymbol{v})\boldsymbol{F}_{base} \tag{11}$$

https://doi.org/10.5194/essd-2026-521
Preprint. Discussion started: 14 July 2026

where $\boldsymbol{F}_{mem}$ indicates the boundary conditions for data assimilation with perturbation, $\boldsymbol{F}_{base}$ indicates the boundary conditions for the numerical simulation, and $\boldsymbol{v}$ indicates perturbations drawn from a normal distribution with a mean of zero and a variance of ξ^2.

The model outputs evaluated in this study, which are explained in Sect. 2.7, were water temperature, salinity, and bottom-layer DO. Accordingly, the placement of perturbations was considered to enhance the accuracy and practical usefulness of the three compartments. According to previous research (Matsuzaki and Inoue, 2022), the boundary conditions to be perturbed and the perturbation amplitudes for temperature and salinity were defined, as shown in Table 1. However, specifying DO perturbations is challenging. In this study, perturbations were applied experimentally to three parameters that empirically exert strong control on bottom-layer DO. First is $\alpha_{DO,const}^{sed}$, which indicates the steady-state oxygen consumption rate of bottom sediments at 0 °C. Second is $\alpha_{H2S,const}^{sed}$, which indicates the H_2S release rate at 0 °C from bottom sediments. Third is $\alpha_{sed,k}$, which indicates the maximum decomposition rate for the k-th fraction.

In this model, a multi-G model that classifies organic matter according to decomposition rate (Westrich and Berner, 1984) was adopted, with k ranging from 1 to 3. In the present study, perturbations were applied at k = 1, which corresponded to the most labile fraction. The values of ξ are summarized in **Table 1**. When a small ensemble of random numbers represents a normal distribution, there is a potential for substantial deviation from the true normal distribution owing to sampling error. In this study, normal random numbers were not employed; instead, each member's value was set to match the cumulative distribution of a normal distribution, so that the normal distribution can be approximated even with a small ensemble. To avoid unintended correlations among boundary conditions, the Fisher–Yates shuffle (Fisher and Yates, 1948) was applied to perform 10,000 replacement attempts, and the boundary conditions and parameters were assigned for each ensemble member using the combination that yielded the lowest correlation.

https://doi.org/10.5194/essd-2026-521
Preprint. Discussion started: 14 July 2026

Table 1. Magnitude of perturbations to boundary conditions and parameters.

Boundary condition/Parameter		Method	ξ
Atmospheric forcing	Air temperature	Equation (10)	1.54 °C
	Wind speed	Equation (11)	0.34
Lateral boundary conditions	Water temperature	Equation (10)	2.16 °C
	Salinity	Equation (10)	0.48
River discharge forcing	River discharge	Equation (11)	0.36
	River water temperature	Equation (10)	2.01 °C
$\alpha_{DO,const}^{sed}$: the steady-state oxygen consumption rate of bottom sediments at 0 °C		Equation (11)	0.50
$\alpha_{H2S,const}^{sed}$: the H_2S release rate from bottom sediments at 0 °C		Equation (11)	0.50
$\alpha_{sed,1}$: the maximum decomposition rate of the most labile fraction		Equation (10)	0.10

2.5 Assimilated observations

Eight in situ observation stations are operating in Ise Bay, and their data were assimilated. In situ water temperature and salinity profiles, along with in situ DO measurements at the bottom layer observed at fixed points, were used for the data assimilation. The data from the five observation stations listed in **Table 2** were assimilated. The assimilated values were observed at 00:00, 06:00, 12:00, and 18:00 and were not averaged. Observation error variance values were set to (1.0 °C)^2 for water temperature, (1.0)^2 for salinity, and (1.0 mg/L)^2 for DO. These water temperature and salinity values were set according to a previous study (Matsuzaki and Inoue, 2022).

The specification of observational error for DO remains a non-trivial challenge in data assimilation studies. Nagano (2025), referring to the measurement-based assessment of Irie et al. (2011), adopted 0.59 mg L^{-1} as a representative effective observation error, with data assimilation performed once per day. In the present study, DO was assimilated every 6 h, which may have enhanced the influence of short-term variability and spatiotemporal representativeness errors. Accordingly, (1.0 mg/L)^2 was adopted as the observation error for DO. A gross error check was performed to control the background quality. The difference between the observed value and the first-guess value was calculated; if this difference exceeded 3 °C for water temperature or 6 for salinity, the observed value was rejected.

2.6 Accuracy validation

The water temperature, salinity, and DO data of the model output were compared with the in situ observation data of water temperature, salinity, and DO profiles observed at fixed points (**Table 2**). Observation data were collected hourly, but assimilations were conducted daily; thus, comparisons were conducted every 6 h. The in situ observation times for the values

https://doi.org/10.5194/essd-2026-521
Preprint. Discussion started: 14 July 2026

were 00:00, 06:00, 12:00, and 18:00, and were not averaged. To evaluate the improvement in accuracy achieved by data assimilation, two model output cases were prepared. Case 1 represents the numerical simulation without data assimilation, and Case 2 represents the results with data assimilation.

Table 2. Assimilated observation data. Observation data from A5 were used for the period June 1, 2022, to December 31, 2022. Observation data from A6, A7, and A8 were used from June 1, 2022, to December 31, 2022.

No.	Station	Latitude (ºN)	Longitude (ºE)	Observation type	Observation depth (m)
A1	Back of Ise Bay	34.926	136.741	Automatic elevating	1.0, 8.0, 16.0, 24.0
A2	Center of Ise Bay	34.669	136.841	Automatic elevating	1.0, 8.0, 16.0, 24.0
A3	Mouth of Ise Bay	34.509	137.018	Fixed	1.0 , 11.8 , and 23.2 from low water level
A4	Western Ise Bay	34.695	136.636	Automatic elevating	1.0, 8.0, 15.0, 22.0
A5	Nakayama Channel	34.623	136.982	Fixed	1.4, 8.2, 12.4
A6	Back of Mikawa Bay	34.743	137.220	Automatic elevating	1.0, 5.0, 8.0, 10.0
A7	Center of Mikawa Bay	34.745	137.072	Automatic elevating	1.0, 5.0, 8.0, 11.0
A8	Mouth of Mikawa Bay	34.675	137.097	Automatic elevating	1.0, 5.0, 10.0, 15.0

The accuracy of the model output was evaluated using the mean error (ME; Equation 12), root-mean-square error (RMSE; Equation 13), correlation coefficient (CC; Equation 14), standard deviation error (SDE; Equation 15), and centered (bias-removed) root-mean-square error (CRMSE; Equation 16):

$$ME = \frac{1}{N}\sum_{i=1}^{N}(m_i - o_i) \tag{12}$$

$$RMSE = \sqrt{\frac{1}{N}\sum_{i=1}^{N}(m_i - o_i)^2} \tag{13}$$

https://doi.org/10.5194/essd-2026-521
Preprint. Discussion started: 14 July 2026

$$CC = \frac{\frac{1}{N}\sum_{i=1}^{N}(m_i - \bar{m})(o_i - \bar{o})}{\sqrt{\frac{1}{N}\sum_{i=1}^{N}(m_i - \bar{m})^2}\sqrt{\frac{1}{N}\sum_{i=1}^{N}(o_i - \bar{o})^2}} \tag{14}$$

$$SDE = \sqrt{\frac{1}{N}\sum_{i=1}^{N}(m_i - \bar{m})^2} - \sqrt{\frac{1}{N}\sum_{i=1}^{N}(o_i - \bar{o})^2} \tag{15}$$

$$CRMSE = \sqrt{\frac{1}{N}\sum_{i=1}^{N}[(m_i - \bar{m}) - (o_i - \bar{o})]^2} \tag{16}$$

where m_i and o_i are model outputs and observations, respectively, N is the number of model outputs and observations, and $\bar{m}$ and $\bar{o}$ are the average values of the model outputs and observations, respectively. The skill scores were calculated for each year, and the average values over the 12-year period are presented in Sect. 3.1.

For qualitative validation, representative stations were selected from Station No. A1–A8. Time series, scatter plots, and isopleth diagrams are presented for the inner parts of Ise Bay and Mikawa Bay (Station Nos. A1 and A6 in Table 2), where hypoxic conditions are relatively pronounced, and for the mouth of Ise Bay (Station No. A3 in Table 2), where hypoxia is relatively weak (Sect. 3.2). We focused on 2021, a year typically characterized by low oxygen levels, in which an event-like resolution of the low oxygen levels, thought to be caused by oceanic water intrusion, was observed. In addition, the spatial distribution of bottom DO from ship-based observations conducted by the Aichi Fisheries Research Institute was compared with that derived from the data assimilation results in Sect. 3.3. The horizontal distribution maps were generated from spatially sparse observations using the Python 3.10.11 library pcolormesh. Tables and figures for all observation stations (Station Nos. A1–A8 in Table 2) are provided in the Supplementary Materials.

3 Results

3.1 Overall statistical performance

First, the reproducibility of the physical fields was examined. For both water temperature (**Figure 2**) and salinity (**Figure 3**), data assimilation improved the overall agreement with observations across all stations and depths, although improvements were not observed at every station. When averaged across all stations and layers for the 12 years, the numerical simulation results for water temperature were substantially improved by data assimilation. The ME decreased from 0.95 °C to 0.31 °C. Similarly, the RMSE decreased from 1.45 °C to 0.77 °C, the CC increased from 0.98 to 0.99, the SDE improved from −0.48 °C to −0.22 °C, and the CRMSE decreased from 0.99 °C to 0.66 °C.

Similar improvements were observed for salinity. Through data assimilation, the ME decreased from 0.16 to 0.09, the RMSE decreased from 0.96 to 0.74, the CC increased from 0.71 to 0.78, and the CRMSE decreased from 0.84 to 0.70. However, salinity SDE was the only metric that did not improve, changing from 0.04 and -0.04.

https://doi.org/10.5194/essd-2026-521
Preprint. Discussion started: 14 July 2026

Next, the reproducibility of DO measurements was examined (**Figure 4**). As with the physical fields, data assimilation improved the overall agreement with observations, although not at all stations. When averaged across all bottom-layer stations over the 12-year period, the DO simulation results showed improved agreement with observations following data assimilation. The ME decreased from −0.35 mg L^{-1} to −0.05 mg L^{-1}. Similarly, the RMSE decreased from 1.32 mg L^{-1} to 1.25 mg L^{-1}, the SDE improved from −0.69 mg L^{-1} to −0.65 mg L^{-1}, and the CRMSE decreased from 1.12 mg L^{-1} to 1.01 mg L^{-1}. The CC remained unchanged at 0.85.

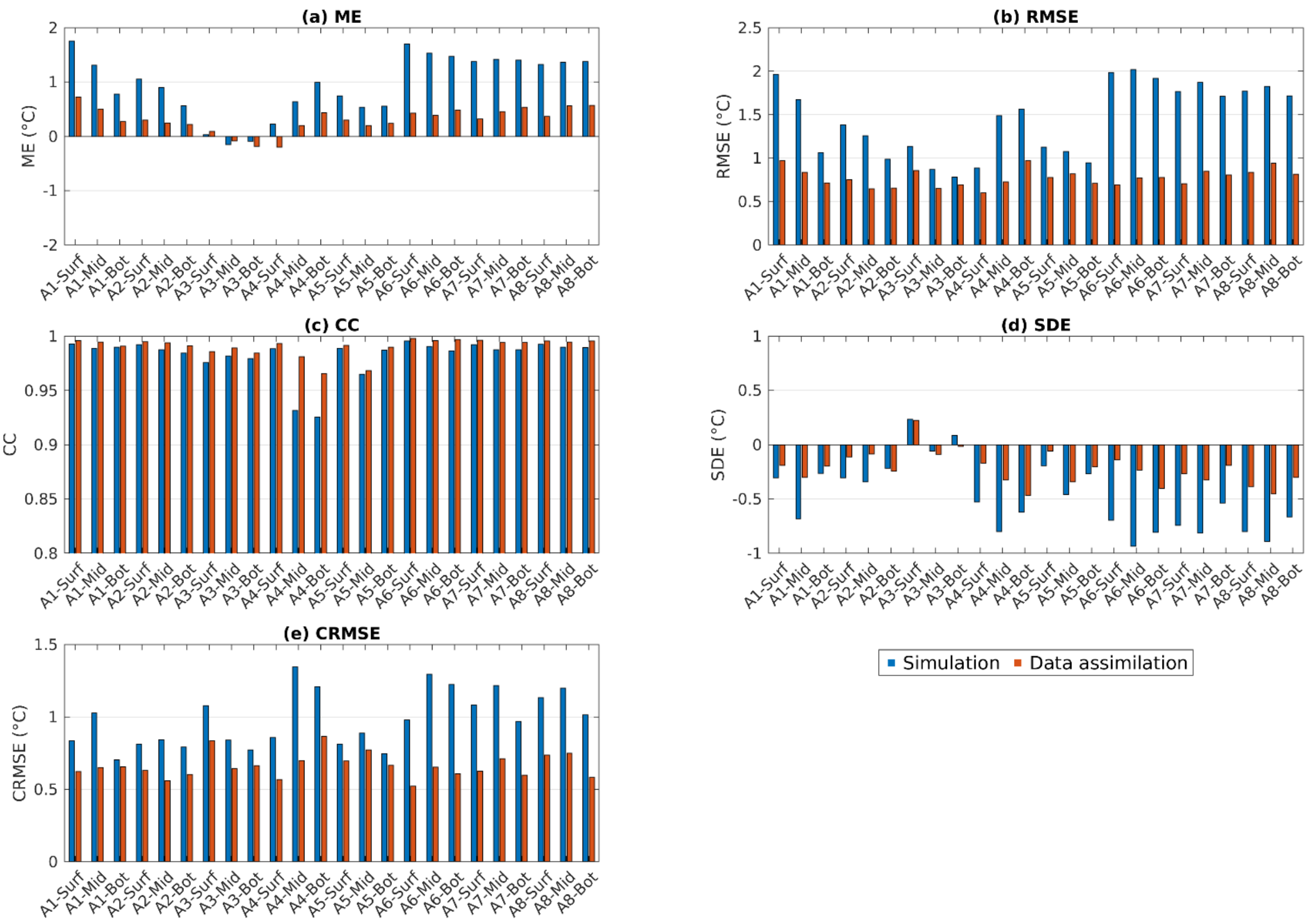

Figure 2: Skill scores of the 12-year numerical simulation and data assimilation results for water temperature at each station (Nos. A1–A8) and each layer (surface layer, middle layer, and bottom layer). (a) Mean error (ME), (b) root-mean-square error (RMSE), (c) correlation coefficient (CC), (d) standard deviation error (SDE), and (e) centered root-mean-square error (CRMSE).

https://doi.org/10.5194/essd-2026-521
Preprint. Discussion started: 14 July 2026

Figure 3: Skill scores of the numerical simulation and data assimilation results for salinity at each station (Nos. A1–A8) and each layer (surface layer, middle layer, and bottom layer). (a) ME, (b) RMSE, (c) CC, (d) SDE, and (e) CRMSE.

https://doi.org/10.5194/essd-2026-521
Preprint. Discussion started: 14 July 2026

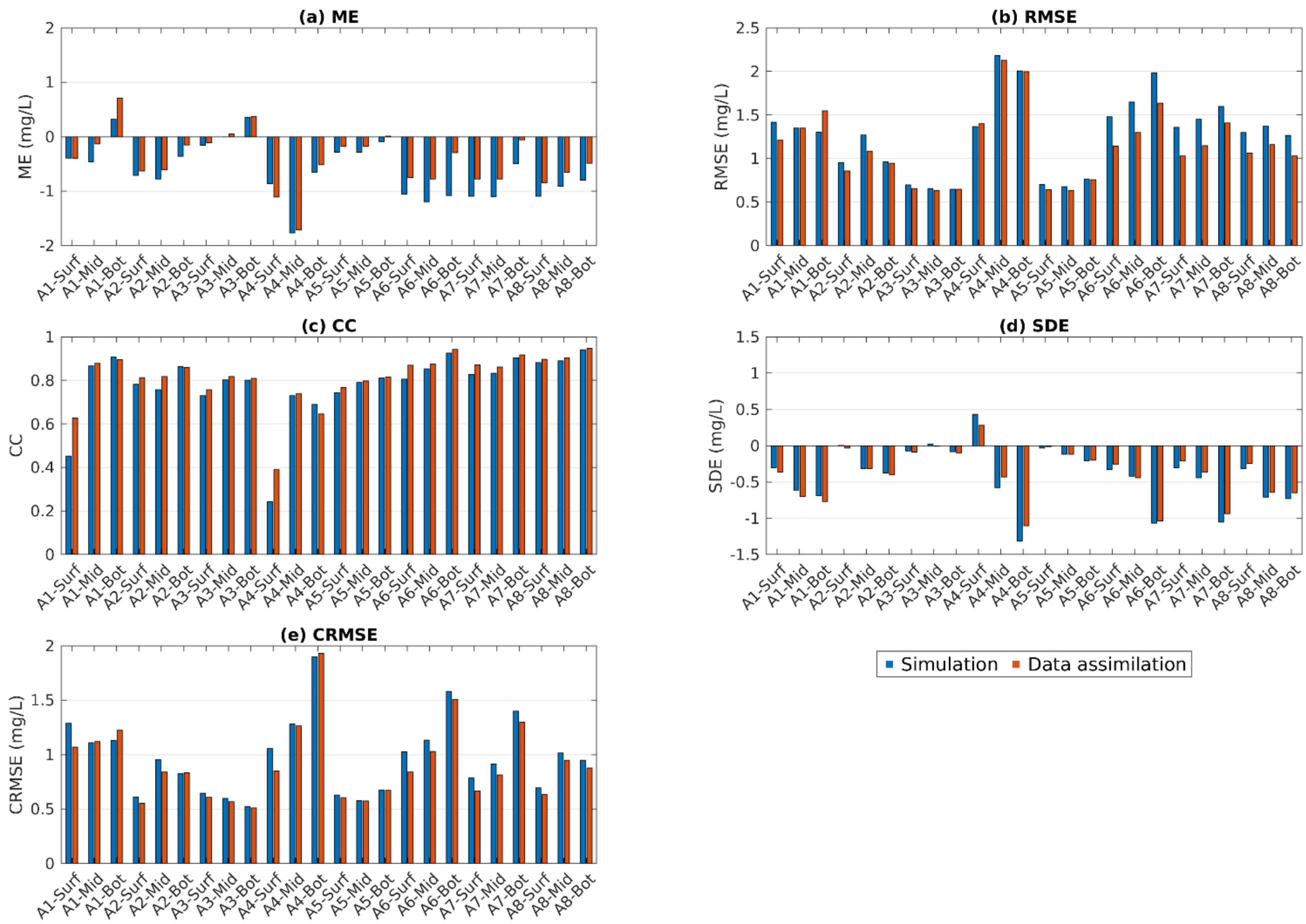

Figure 4: Skill scores of the numerical simulation and data assimilation results for DO at each station (Nos. A1–A8) and each layer (surface layer, middle layer, and bottom layer). (a) ME, (b) RMSE, (c) CC, (d) SDE, and (e) CRMSE.

3.2 Temporal and vertical structure variability at representative stations

First, we describe the results for the back of Mikawa Bay (Station No. A6), where hypoxic conditions are relatively pronounced. The seasonal variability in water temperature, as well as the timing of decreases and increases in salinity, was qualitatively consistent across all layers (surface, middle, and bottom) (Figure 5Figure 6). The scatter plots of water temperature and salinity show that the data assimilation results are close to the 1:1 line, indicating good agreement with the observations.

Bottom-layer DO also reproduced seasonal variability, including the development of hypoxia during summer and its recovery in autumn (Figure 7). The timing of the onset and breakdown of stratification was also well captured. The scatter plots of DO show that the data assimilation results are close to the 1:1 line, indicating good agreement with the observations.

https://doi.org/10.5194/essd-2026-521
Preprint. Discussion started: 14 July 2026

Open Access Earth System Science Data Discussions

The vertical stratification structure (**Figure 8**) is well represented, with the development of a strong thermocline during summer. Hypoxic conditions developed in the bottom layer during the stratified periods, which is consistent with observations. The data assimilation results successfully reproduced the formation and persistence of bottom-layer hypoxia.

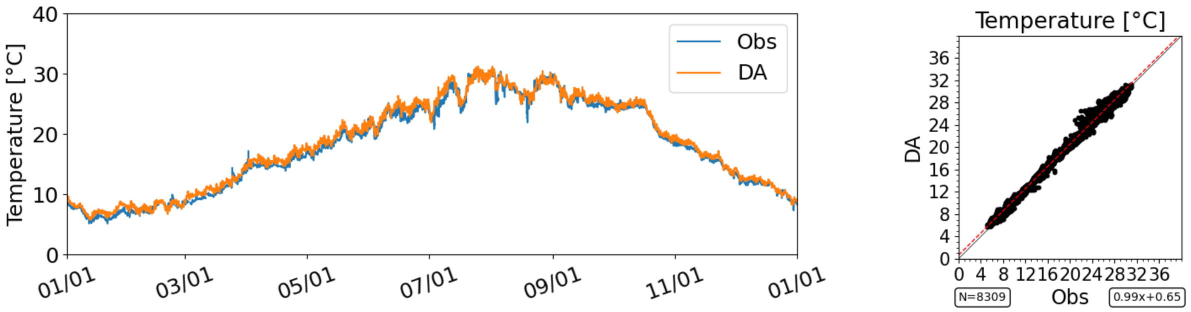

(a) Surface layer

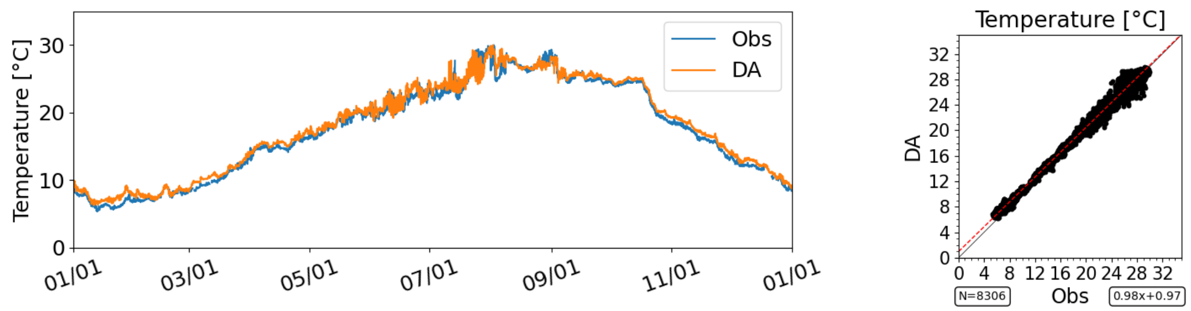

(b) Middle layer

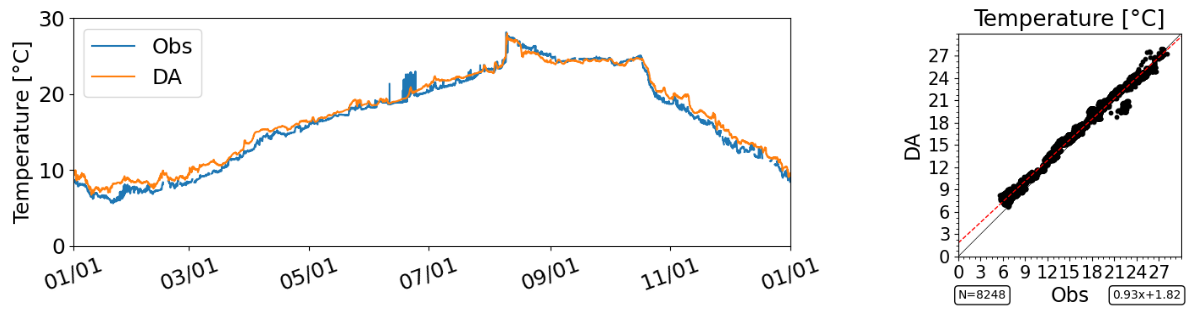

(c) Bottom layer

Figure 5: Time series and scatter plot of water temperature at the back of Mikawa Bay (Station No. A6) for 2021 °

https://doi.org/10.5194/essd-2026-521
Preprint. Discussion started: 14 July 2026

Open Access Earth System Science Data Discussions

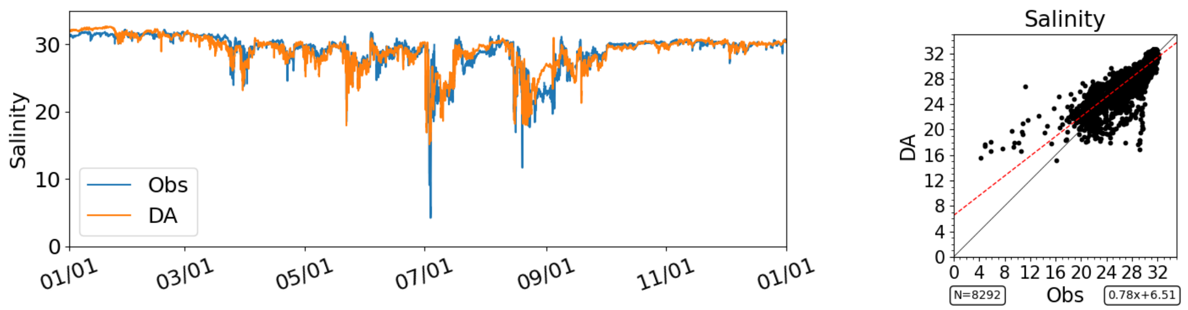

(a) Surface layer

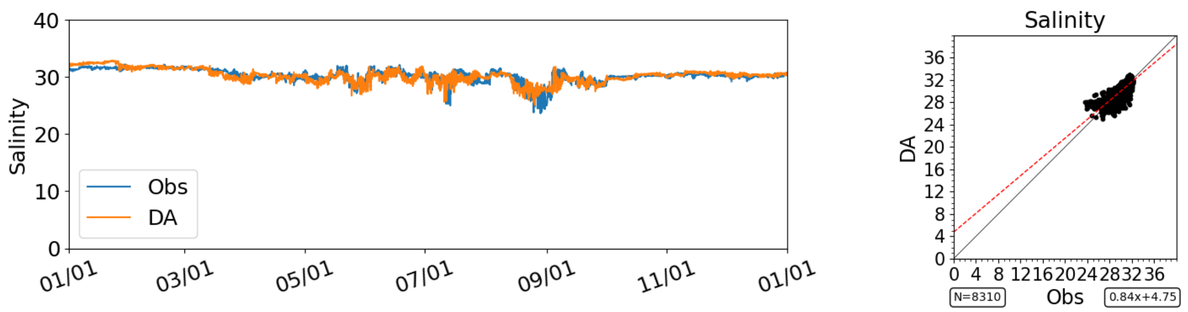

(b) Middle layer

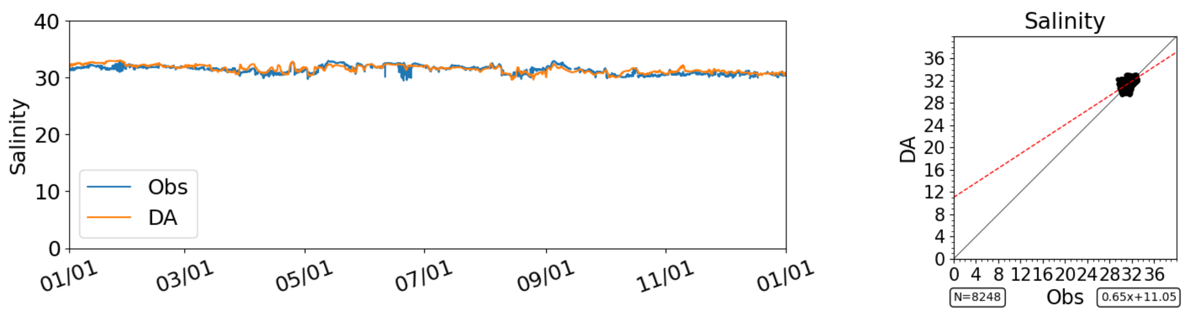

(c) Bottom layer

Figure 6: Time series and scatter plot of salinity at the back of Mikawa Bay (Station No. A6) for 2021

https://doi.org/10.5194/essd-2026-521
Preprint. Discussion started: 14 July 2026

Open Access Earth System Science Data Discussions

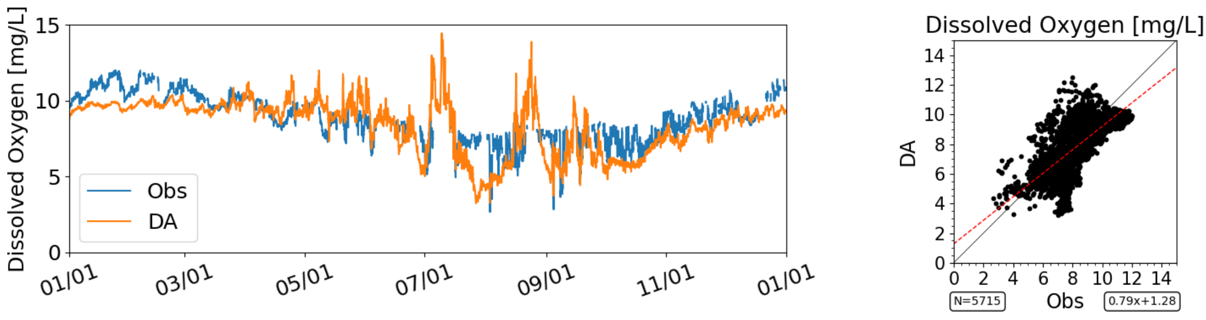

(a) Surface layer

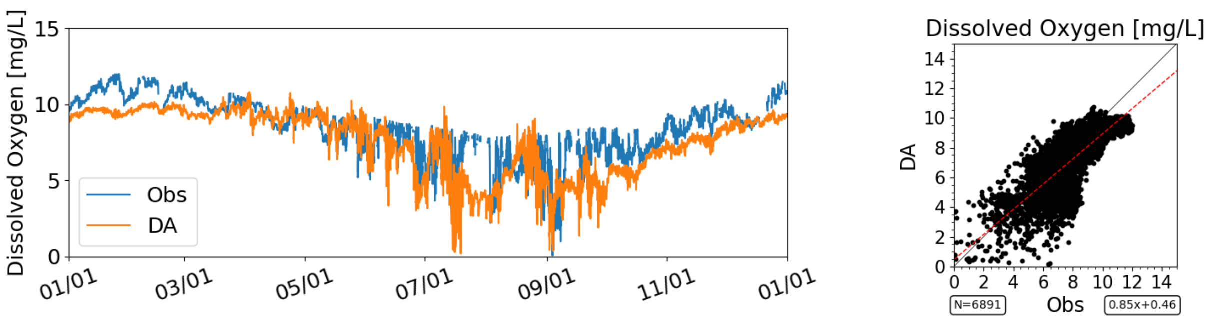

(b) Middle layer

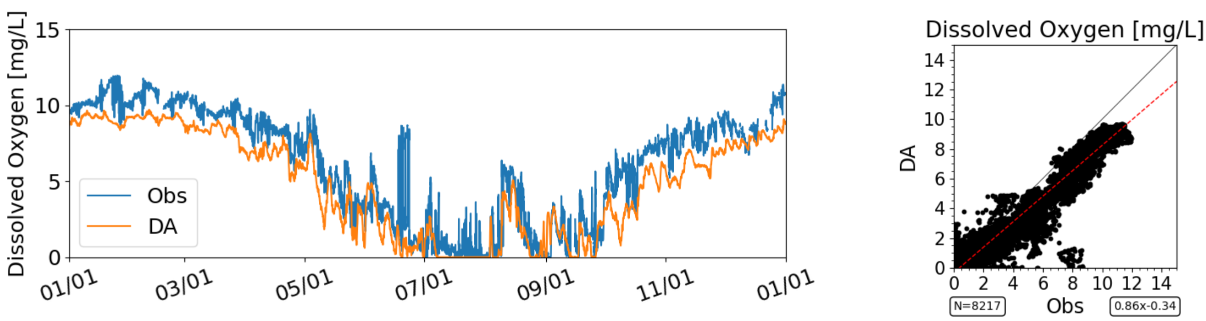

(c) Bottom layer

Figure 7: Time series and scatter plot of DO at the back of Mikawa Bay (Station No. A6) for 2021

https://doi.org/10.5194/essd-2026-521
Preprint. Discussion started: 14 July 2026

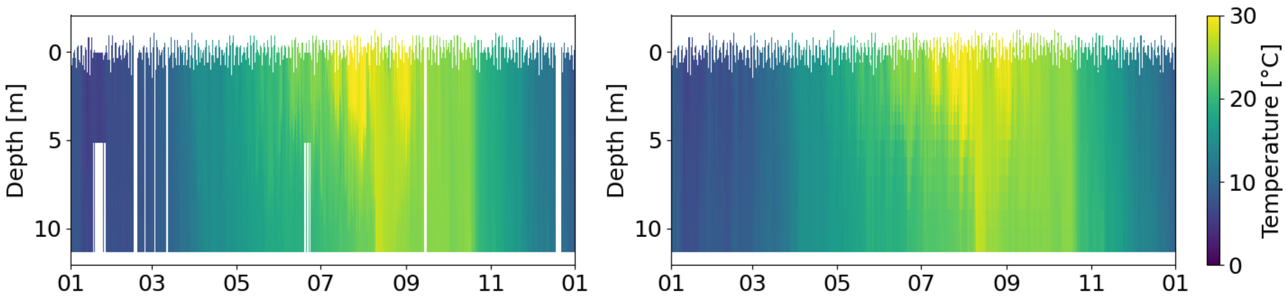

(a) Water temperature

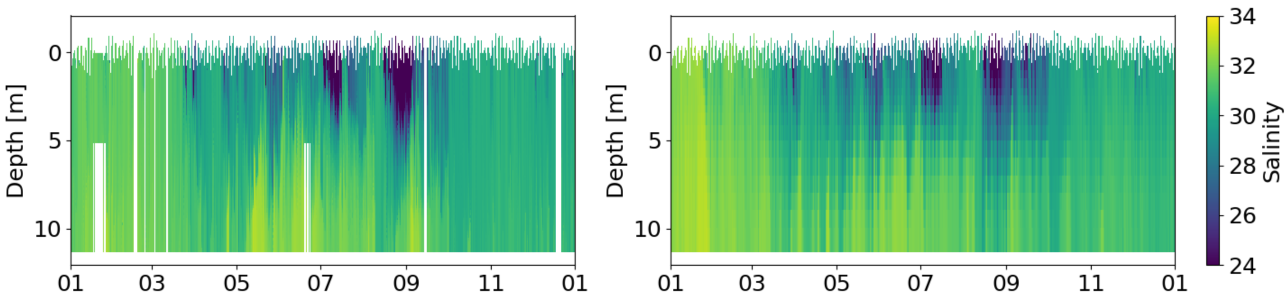

(b) Salinity

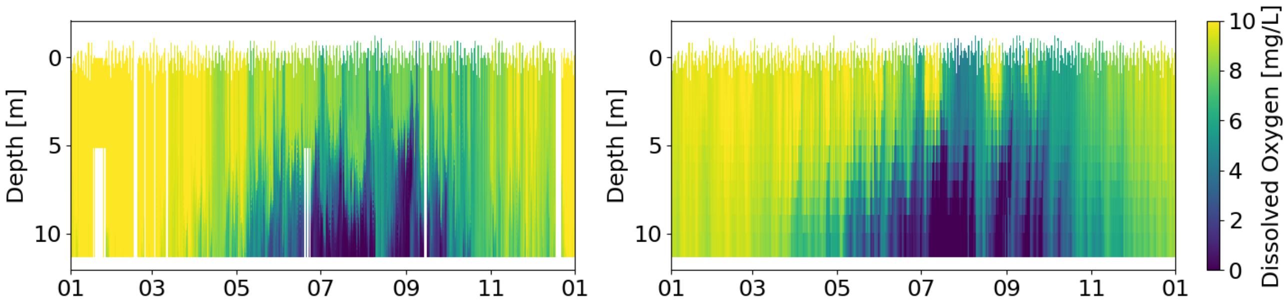

(c) DO

Figure 8: Isopleths of observed (left) and data-assimilated (right) results at the back of Mikawa Bay (Station No. A6) for 2021

Next, we considered the back of Ise Bay (Station No. A1), where hypoxic conditions are also observed but are generally less severe than those in the inner Mikawa Bay. Seasonal patterns of water temperature and the timing of salinity variations were consistently reproduced across all layers (surface, middle, and bottom) (
Figure 9 and Figure 10). The agreement between the data assimilation results and the observations was further supported by the scatter plots, which showed a close alignment with the 1:1 line.

DO in the bottom layer exhibited a similar seasonal cycle, with lower DO levels occurring in summer and recovery toward autumn (Figure 11). The transition between the stratified and mixed conditions was reasonably captured in terms of both timing and magnitude. The scatter plots indicate that the assimilated results corroborate the observed DO values.

https://doi.org/10.5194/essd-2026-521
Preprint. Discussion started: 14 July 2026

The vertical stratification structure (Figure 12) was also reproduced, including the formation of a thermocline during summer. Under these stratified conditions, the development of bottom-layer hypoxia was represented in a manner consistent with observations. Overall, the data assimilation results provide a reliable representation of the temporal variability and vertical distribution of the bottom-layer DO in inner Ise Bay.

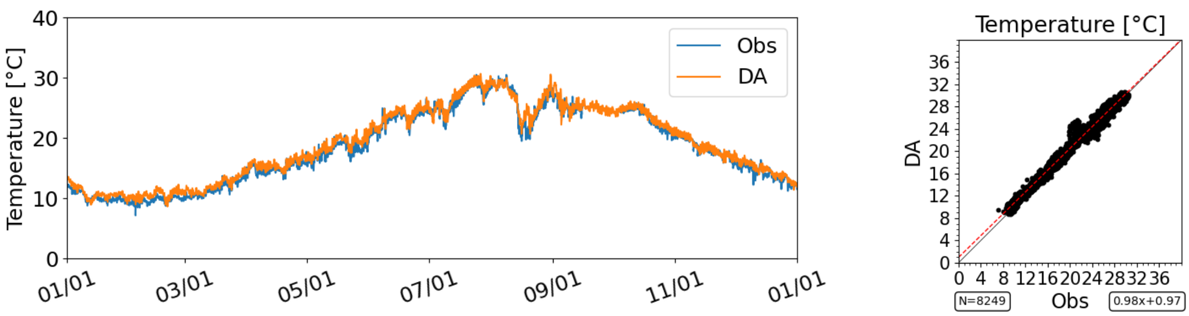

(a) Surface layer

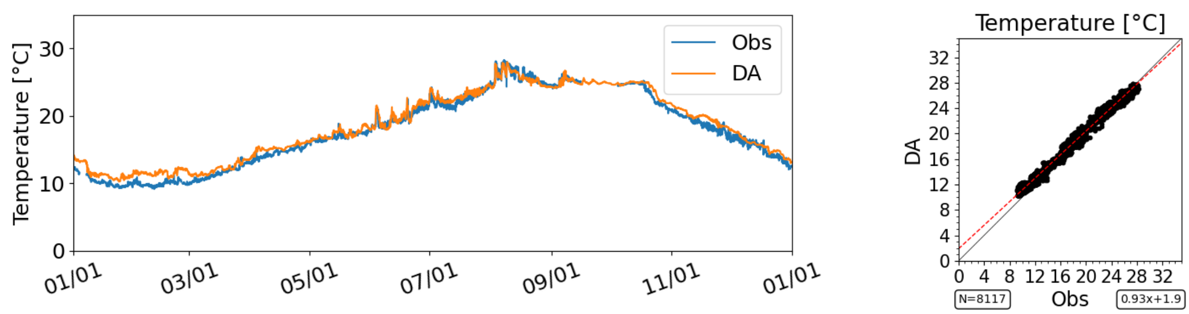

(b) Middle layer

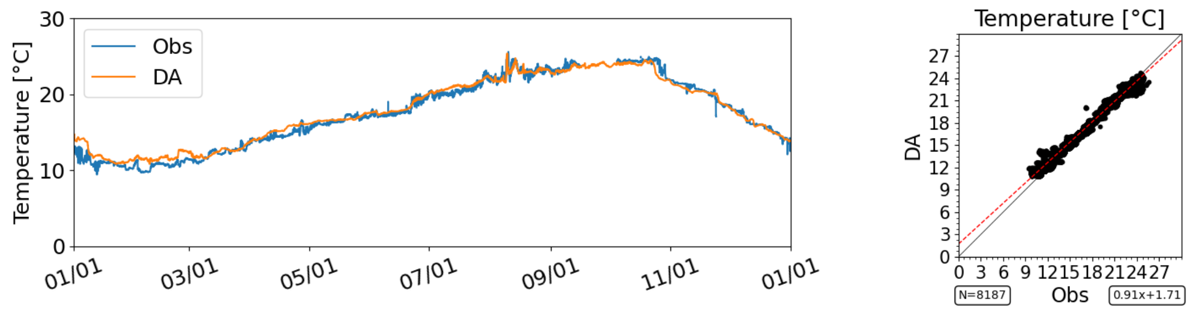

(c) Bottom layer

Figure 9: Time series and scatter plot of water temperature at the back of Ise Bay (Station No. A1) for 2021

https://doi.org/10.5194/essd-2026-521
Preprint. Discussion started: 14 July 2026

Open Access Earth System Science Data Discussions

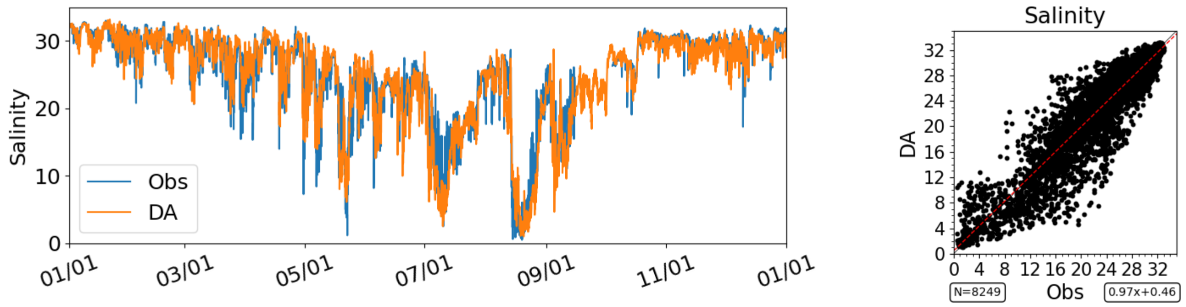

(a) Surface layer

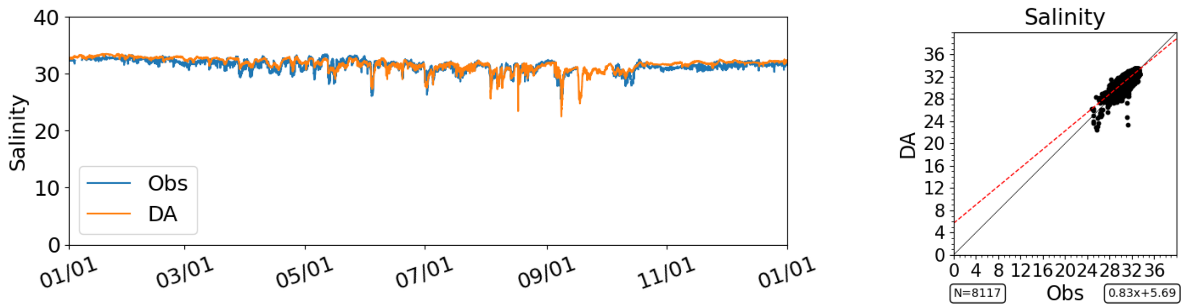

(b) Middle layer

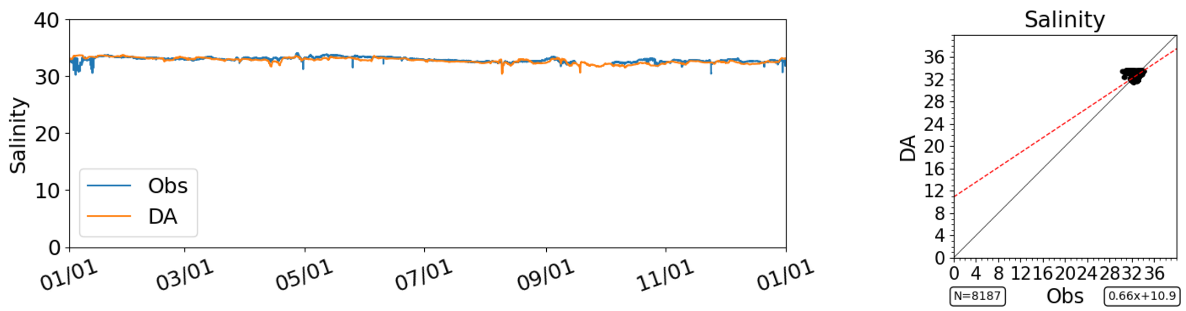

(c) Bottom layer

Figure 10: Time series and scatter plot of salinity at the back of Ise Bay (Station No. A1) for 2021

https://doi.org/10.5194/essd-2026-521
Preprint. Discussion started: 14 July 2026

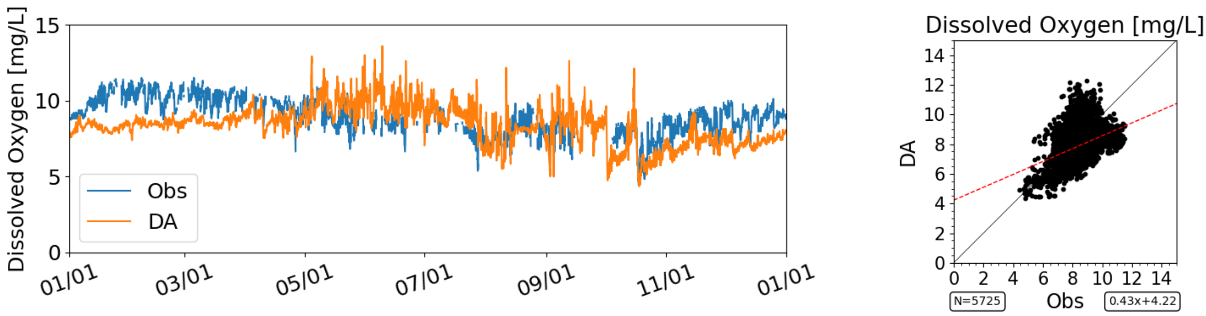

(a) Surface layer

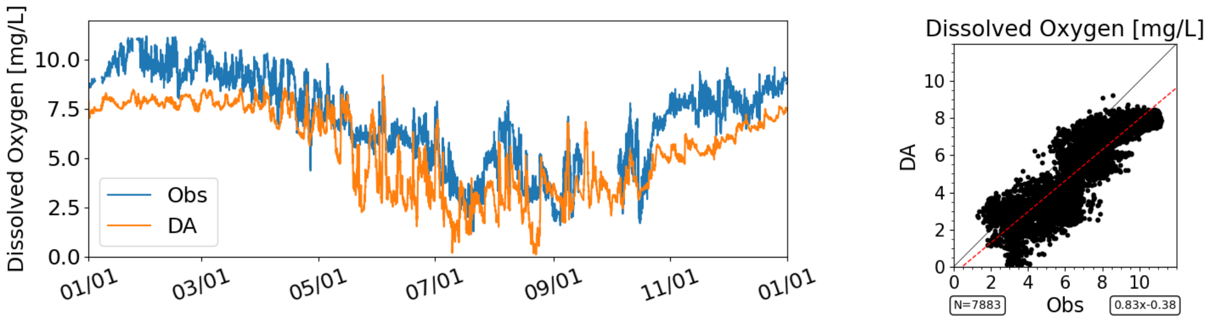

(b) Middle layer

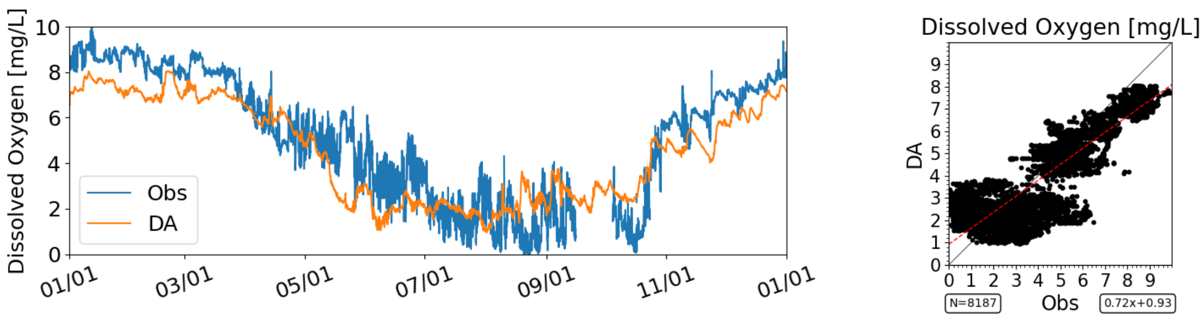

(c) Bottom layer

Figure 11: Time series and scatter plot of DO at the back of Ise Bay (Station No. A1) for 2021.

https://doi.org/10.5194/essd-2026-521
Preprint. Discussion started: 14 July 2026

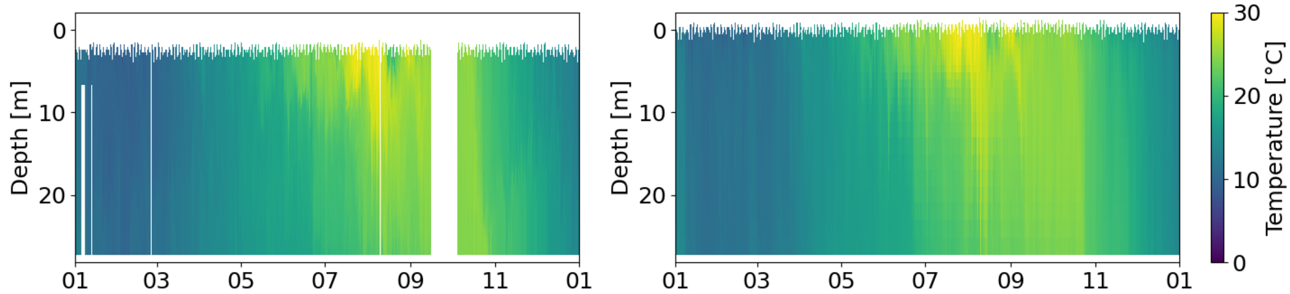

(a) Water temperature

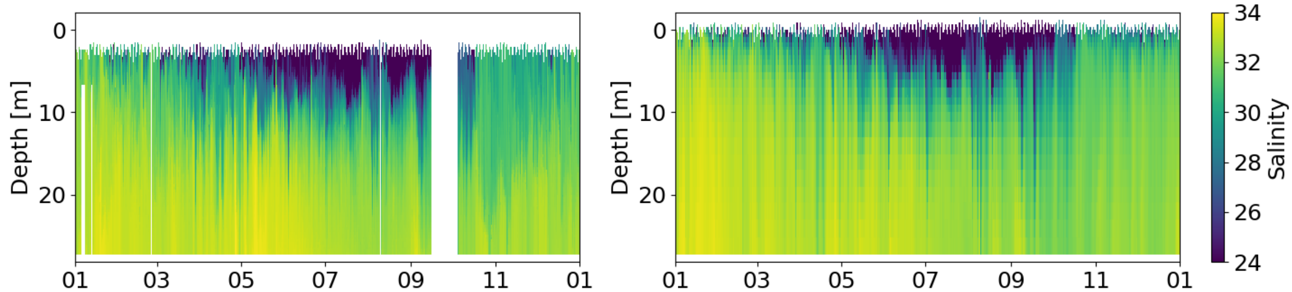

(b) Salinity

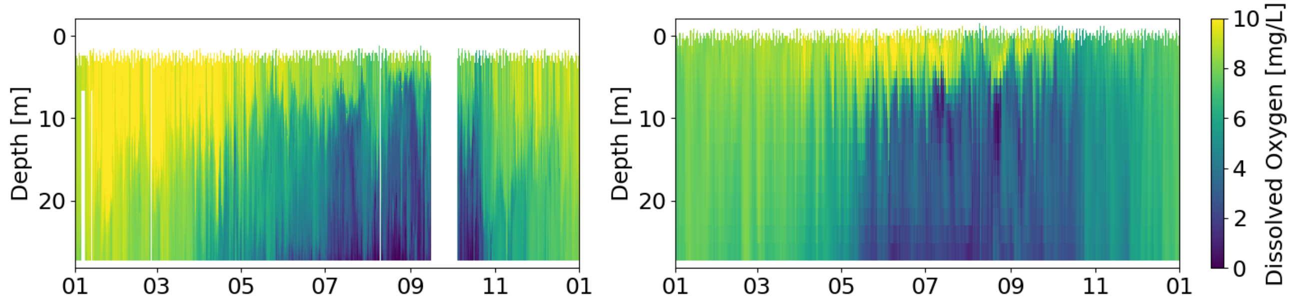

(c) DO

Figure 12: Isopleths of observed (left) and data-assimilated (right) results at the back of Ise Bay (Station No. A6) for 2021.

Finally, we examined the mouth of Ise Bay (Station No. A3), where hypoxic conditions were not observed, and DO levels remained relatively higher than in the inner-bay regions. The seasonal variability in water temperature and timing of salinity changes were consistently reproduced across the surface, middle, and bottom layers (**Figure 13** and Figure 14). The scatter plots further demonstrate good agreement between the data assimilation results and observations, with the data points clustered near the 1:1 line.

https://doi.org/10.5194/essd-2026-521
Preprint. Discussion started: 14 July 2026

The DO in the bottom layer also exhibited a distinct seasonal cycle, although the values did not reach hypoxic levels. DO concentrations tended to decrease during summer and recover toward autumn (Figure 15), and these temporal variations were well represented by the data assimilation results. The model captured the transition between stratified and well-mixed conditions in terms of both timing and overall magnitude. The scatter plots confirm that the assimilation results are generally consistent with the observed DO values. Overall, the data assimilation results provide a robust representation of the temporal variability and vertical structure of bottom-layer DO under non-hypoxic conditions at the bay mouth.

https://doi.org/10.5194/essd-2026-521
Preprint. Discussion started: 14 July 2026

Open Access Earth System Science Data Discussions

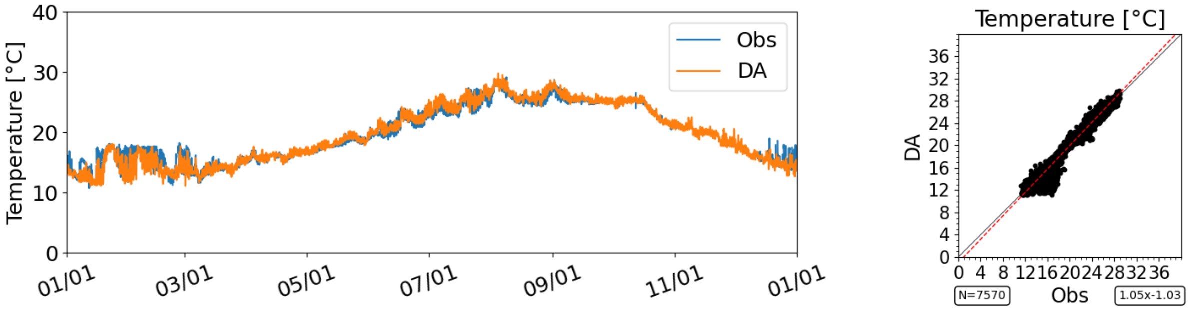

(a) Surface layer

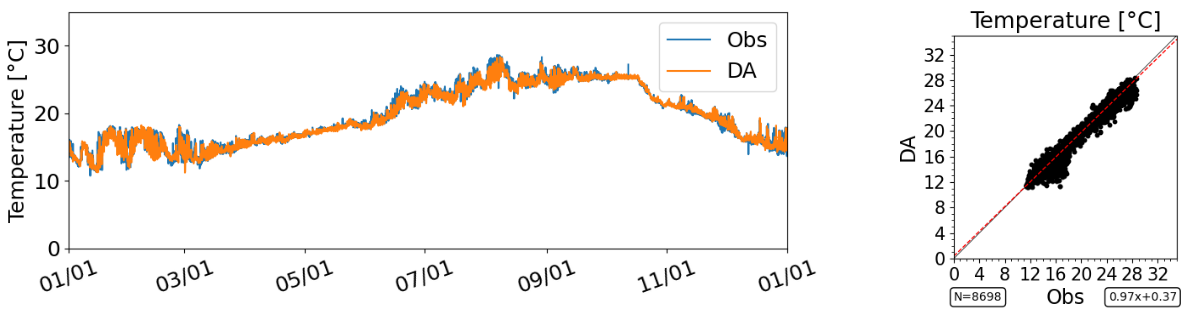

(b) Middle layer

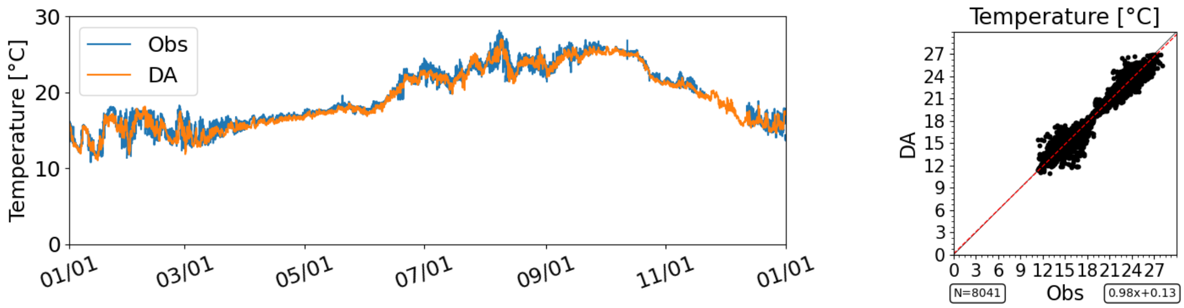

(c) Bottom layer

365 **Figure 13: Time series and scatter plot of water temperature at the mouth of Ise Bay (Station No. A3) for 2021**

https://doi.org/10.5194/essd-2026-521
Preprint. Discussion started: 14 July 2026

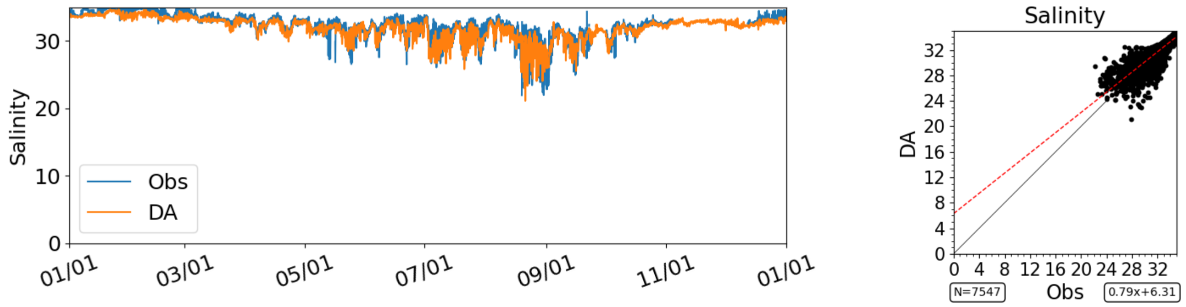

(a) Surface layer

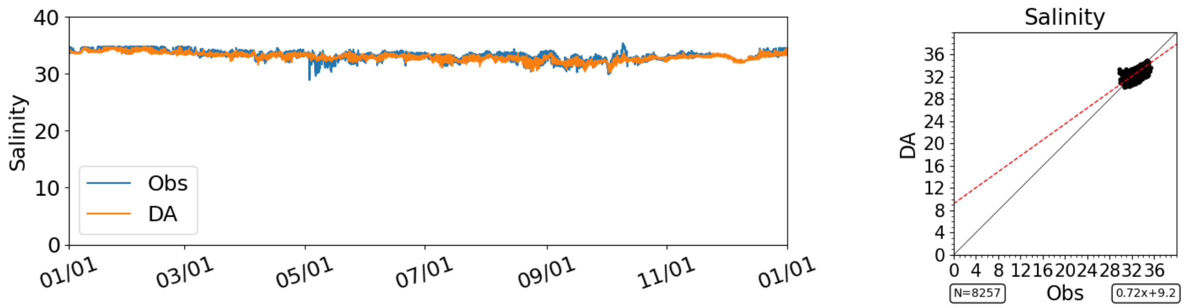

(b) Middle layer

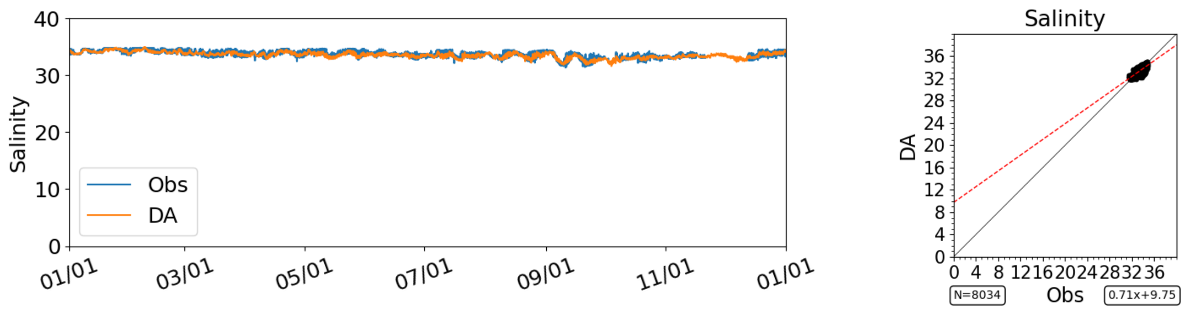

(c) Bottom layer

Figure 14: Time series and scatter plot of salinity at the mouth of Ise Bay (Station No. A3) for 2021

https://doi.org/10.5194/essd-2026-521
Preprint. Discussion started: 14 July 2026

Open Access Earth System Science Data Discussions

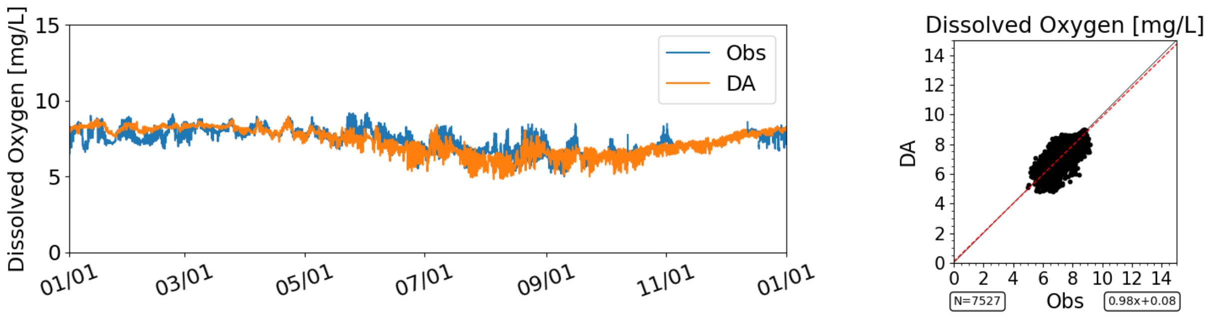

(a) Surface layer

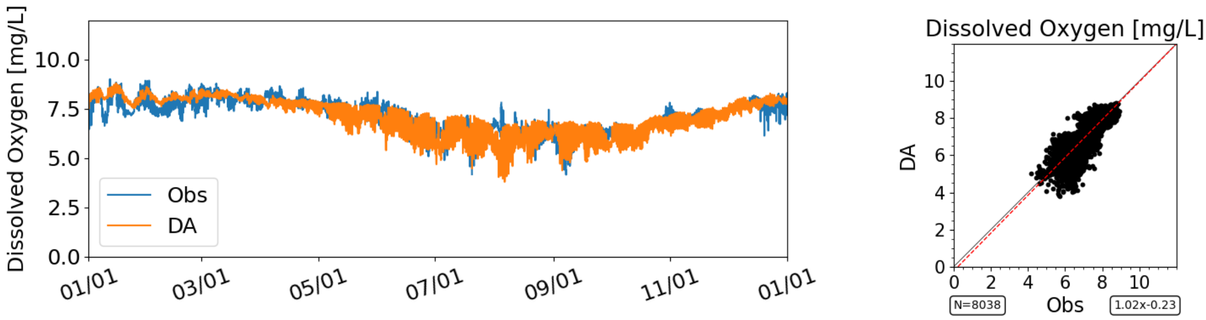

(b) Middle layer

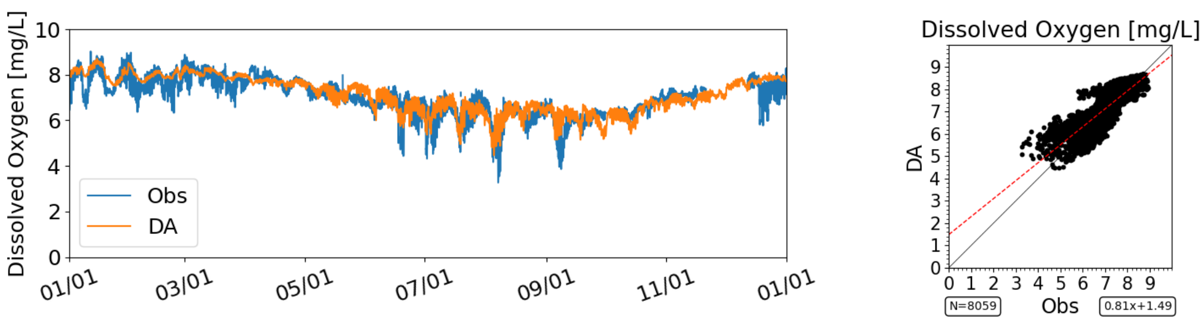

(c) Bottom layer

Figure 15: Time series and scatter plot of DO at the mouth of Ise Bay (Station No. A3) for 2021

3.3 Spatial distribution snapshot

Figure 16 Figure **17** show the horizontal distributions of the observed data and the data assimilation results for the surface and bottom layers, respectively. Although the observational data were spatially sparse, the data assimilation results reproduced the inflow of high-salinity water from the open ocean and the outflow of low-salinity water along the western coast of Ise Bay. These observations are generally consistent with these patterns.

https://doi.org/10.5194/essd-2026-521
Preprint. Discussion started: 14 July 2026

Water temperature and surface DO also exhibited spatial distributions reflecting the influence of both inner bay and open ocean water masses, similar to salinity. In the bottom layer, the data assimilation results indicated the intrusion of high-DO water from the eastern offshore region, resulting in a clear east–west DO gradient within Ise Bay. A similar spatial pattern was also observed in the measurements. The intrusion of high-DO water masses was further supported by the distributions of bottom-layer temperature and salinity, showing an overall consistency between the data assimilation results and observations. However, some discrepancies remained in the absolute DO values. For example, at 11:00 on August 6, the data assimilation results slightly underestimated DO relative to the observations. These results indicate that the data assimilation framework effectively reconstructs mesoscale spatial structures in both the physical and biogeochemical fields, despite the limited availability of observational data.

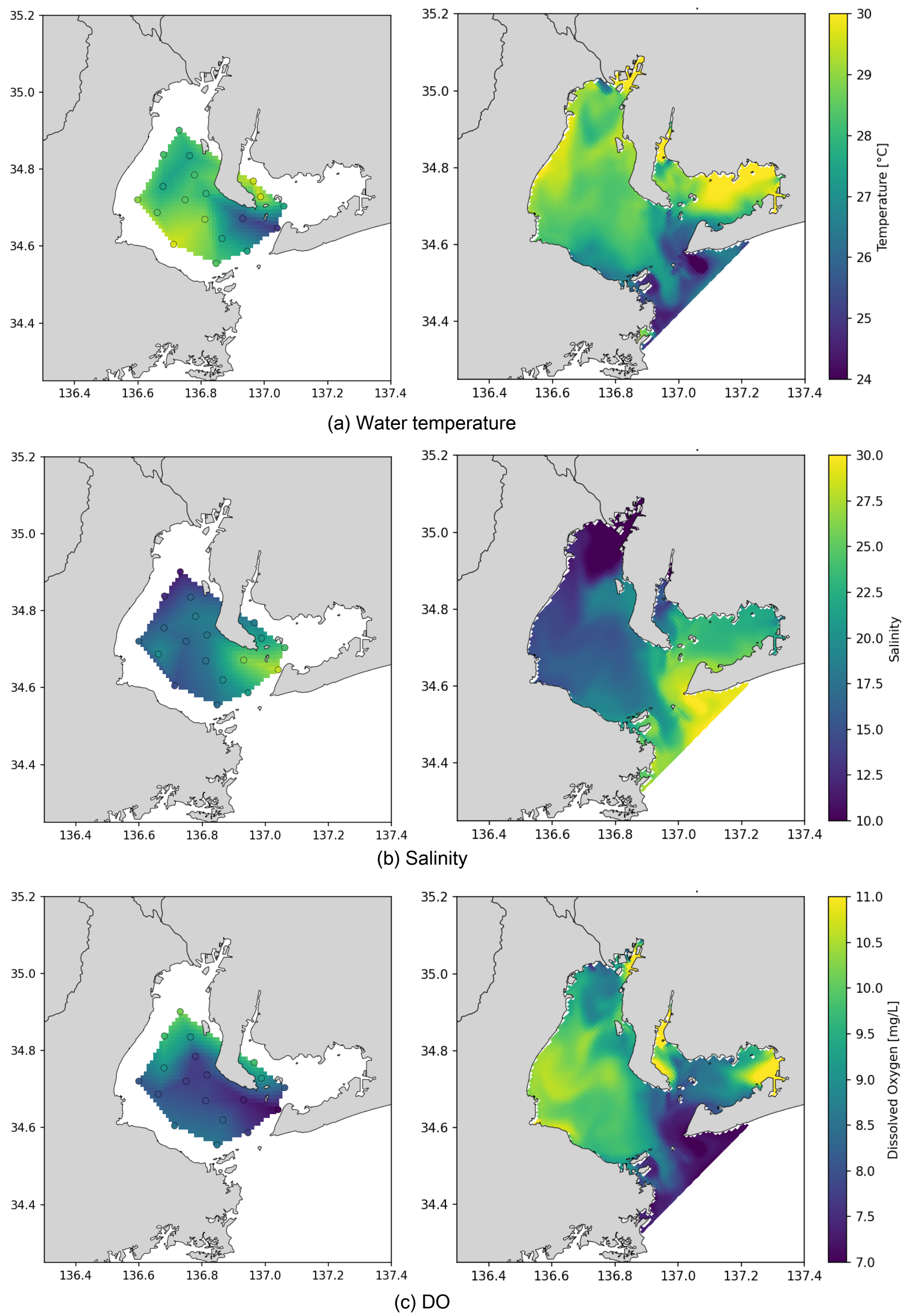

Figure 16: Horizontal distributions of observed (left) and data-assimilated (right) results in the surface layer at 11:00 AM on August 6, 2020. (a) Water temperature, (b) salinity, and (c) DO. Circles in the left panels denote observation locations.

https://doi.org/10.5194/essd-2026-521
Preprint. Discussion started: 14 July 2026

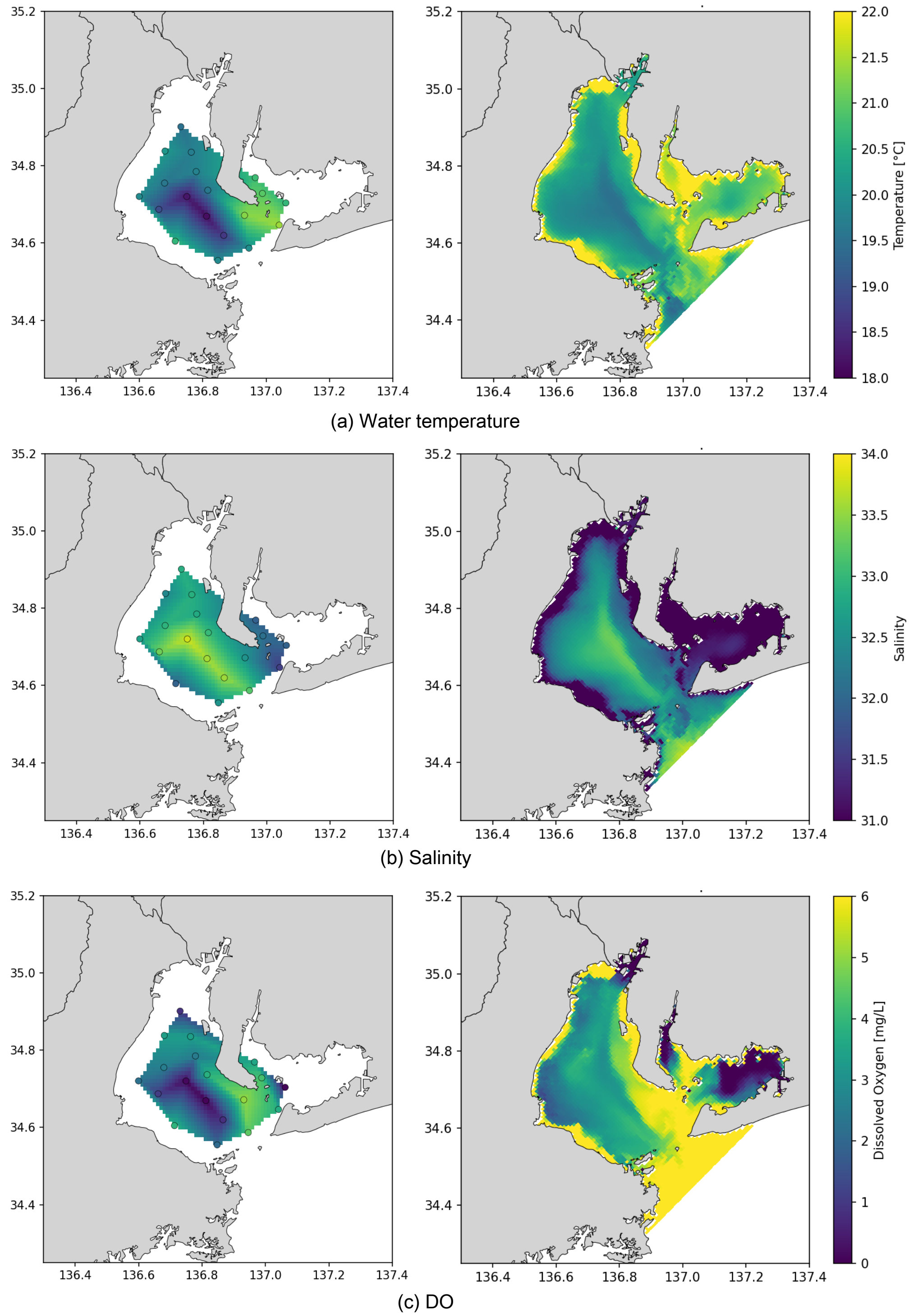

390 **Figure 17: Horizontal distributions of observed (left) and data-assimilated (right) results in the bottom layer (1.0 m above the seabed) at 11:00 AM on August 6, 2020. (a) Water temperature, (b) salinity, and (c) DO. Circles in the left panels denote observation points.**

https://doi.org/10.5194/essd-2026-521
Preprint. Discussion started: 14 July 2026

4 Discussion

The IBRA dataset was developed in this study to construct a reanalysis dataset with three key features. First, unlike many previous reanalysis datasets that rely primarily on satellite observations, IBRA assimilates continuous in situ measurements throughout the water column, including high-frequency DO observations, thereby improving the representation of subsurface dynamics. Second, the 6 h assimilation cycle enables the dataset to resolve short-term variability driven by tidal processes, which are a dominant control on coastal transport and mixing. Third, spatially coherent corrections are applied over the entire bay using an ensemble Kalman filter, ensuring spatial consistency of both physical and biogeochemical fields while avoiding artificial discontinuities often associated with simpler assimilation approaches. Based on the results presented in Section 3, the extent to which these objectives have been achieved is discussed below.

4.1 Assimilation of subsurface observations

The statistical metrics for water temperature, salinity, and DO show improvement across the entire bay (Figure 2–Figure 4), indicating that the assimilation of water-column observations functions effectively. This represents a significant advancement for this study, as many previous reanalysis datasets have relied primarily on satellite observations, which provide only surface information. By incorporating continuous in situ measurements throughout the water column, IBRA achieves a more realistic representation of subsurface physical and biogeochemical processes.

4.2 High-frequency data assimilation

In this study, the performance of the 12-year reanalysis dataset was evaluated primarily in terms of long-term accuracy rather than short-term variability. Previous work (Mizuguchi et al., 2025) demonstrated that the assimilation of observations at 6-h intervals effectively improves physical fields in coastal environments influenced by tidal currents.
Consistent with this finding, an improvement in the correlation coefficient (CC) of salinity from 0.71 to 0.78 is observed in the present study (**Figure 3**), suggesting that the assimilation framework contributes to improved temporal representation. Therefore, the present dataset, which adopts a similar high-frequency assimilation strategy, is expected to provide an enhanced representation of short-term variability. The ability to capture rapid changes associated with stratification, mixing, and water mass exchange is partly attributable to the 6-h data assimilation cycle. However, a more detailed evaluation of short-term processes remains a subject for future study.

4.3 Spatial consistency

From the one-year isopleth diagrams in Section 3.2 (Figure 8 andFigure 12) and the horizontal distribution snapshots in Section 3.3 (**Figure 16** andFigure 17), no artificial discontinuities or unrealistic density inversions in salinity and temperature were observed. This is also confirmed in the Supplementary Materials, which present isopleth diagrams for all stations over the

https://doi.org/10.5194/essd-2026-521
Preprint. Discussion started: 14 July 2026

entire 12-year period. These results suggest that the data assimilation framework provides spatially consistent corrections throughout the bay, avoiding localized or discontinuous adjustments that are often associated with simpler assimilation approaches. Although the effect of applying spatially coherent corrections over the entire domain cannot be quantified in a strict sense, the results qualitatively indicate that this approach is effective.

5 Data description and access

5.1 Dataset overview

The IBRA dataset provides a 12-year (2011–2022) high-resolution reanalysis of the ocean circulation and biogeochemical variables for Ise Bay, Japan. The dataset is based on a coupled ocean circulation with an ecosystem model and a data assimilation system that incorporates in situ observations of water temperature, salinity, and DO. The dataset has an hourly temporal resolution and resolves the full water column using 38 vertical layers over a horizontal grid of 85 × 85 cells. All timestamps are provided in Japan Standard Time (JST; UTC+9). Data assimilation is performed every 6 h (00, 06, 12, and 18 JST); these time steps correspond to the analysis states, whereas the intermediate hourly data represent forward simulations initialized from the preceding assimilation cycle. This temporal structure allows the dataset to represent both short-term variability, including tidal processes, and longer-term seasonal dynamics. In particular, the inclusion of bottom-layer DO observations enables a detailed assessment of hypoxic conditions in enclosed coastal environments.

5.2 Variables and file structure

The dataset includes three primary variables: water temperature (°C), salinity, and DO (mol m^{-3}), provided at all grid points and vertical layers. In addition to these variables, the dataset includes water level (m) and horizontal velocity components in the x and y directions (m s^{-1}). Although these variables were not evaluated in this study, they are provided for potential users' benefit. The data were distributed in the NetCDF4 format and organized as annual files (one file per year). Each file contains multidimensional arrays with dimensions of time, horizontal coordinates, and vertical layers. Standard metadata, including variable definitions, physical units, and coordinate systems, are included in accordance with common oceanographic data conventions.

5.3 Usage notes and limitations

The IBRA dataset is designed to enable a more accurate representation of subsurface physical and biogeochemical processes, particularly bottom-layer DO. However, this study has some limitations. The accuracy of the dataset may vary depending on its location and environmental conditions. In particular, discrepancies persist in the absolute DO values during periods of rapid variability, such as mixing events. Therefore, users should consider these uncertainties when applying the dataset to quantitative analyses. Despite these limitations, the dataset provides a robust and dynamically consistent representation of the

https://doi.org/10.5194/essd-2026-521
Preprint. Discussion started: 14 July 2026

Open Access Earth System Science Data Discussions

physical and biogeochemical variability in an enclosed coastal system. It is expected to be a valuable resource for scientific research and environmental assessment.

6 Conclusions

The IBRA dataset provides a high-resolution, long-term reanalysis of coastal circulation and biogeochemical conditions in a highly enclosed coastal environment. With hourly temporal resolution, full water-column coverage, and assimilation of in situ observations, it is well suited for a wide range of scientific and practical applications. Key features include spatially consistent corrections across the bay, high-frequency data assimilation capable of resolving tidal-scale variability, and incorporation of continuous water-column observations, including dissolved oxygen (DO), enabling an improved representation of subsurface processes. One of the primary applications of IBRA is assessing hypoxic conditions in enclosed coastal waters. The dataset enables detailed analysis of the temporal evolution, spatial distribution, and interannual variability of bottom-layer DO, providing insights into the mechanisms of hypoxia formation and dissipation. IBRA can also support evaluations of compliance with environmental quality standards based on bottom-layer DO concentrations, which are being increasingly implemented in Japan. In addition, the dataset can be used to investigate physical–biogeochemical interactions in coastal environments, including the effects of stratification, tidal forcing, and water mass exchange between the open ocean and inner bays. The high temporal resolution and frequent data assimilation allow the dataset to capture short-term variability, such as episodic mixing events and rapid DO changes associated with oceanic intrusions. The IBRA dataset is also valuable for model validation, data-driven analyses, and providing boundary or initial conditions for regional and local modeling studies. Furthermore, it may serve as a valuable resource for stakeholders involved in coastal management, environmental policy, and ecosystem assessment. Despite these advantages, some limitations remain. While the dataset reproduces the overall variability and spatial structure of physical and biogeochemical fields, discrepancies persist in the absolute values of DO under certain conditions, particularly during periods of rapid variability, which cannot be fully captured by the circulation model. These uncertainties should be considered when applying the dataset to quantitative analyses. In summary, IBRA provides a comprehensive and dynamically consistent representation of coastal physical and biogeochemical conditions in Ise Bay. By combining high-resolution modeling with in situ data assimilation, the dataset fills an important gap in coastal reanalysis products and is expected to contribute to both scientific research and environmental management.

Data availability

The IBRA dataset is publicly available via Zenodo at: https://doi.org/10.5281/zenodo.19808667 (Matsuzaki et al., 2026). The dataset was distributed as yearly NetCDF files from 2011 to 2022. Detailed instructions for downloading and using the data, including file descriptions and metadata, are provided in the repository. The dataset was released under the Creative Commons Attribution 4.0 International (CC BY 4.0) license.

https://doi.org/10.5194/essd-2026-521
Preprint. Discussion started: 14 July 2026

Open Access Earth System Science Data Discussions

Author contributions

Yoshitaka Matsuzaki: Conceptualization, Funding acquisition, Methodology, Project administration, Resources, Writing (original draft preparation); Hayato Mizuguchi: Investigation, Validation, Visualization; Tetsunori Inoue: Conceptualization, Supervision

Competing interests

The authors declare that they have no conflicts of interest.

Acknowledgments

The authors thank Dr. Yoshiyuki Nakamura, Dr. Kosuke Ito, and Dr. Toshinori Okuda for their valuable comments and suggestions. The observational data used in this study were provided by the Chubu Regional Development Bureau of the Ministry of Land, Infrastructure, Transport and Tourism and the Aichi Fisheries Research Institute. The authors thank Editage (www.editage.jp) for English language editing.

Financial support

This study was supported by the Environment Research and Technology Development Fund [Grant No.: JPMEERF20221R01] of the Environmental Restoration and Conservation Agency, provided by the Ministry of the Environment of Japan, the Joint Usage/Research Center for Interdisciplinary Large-scale Information Infrastructures (JHPCN) of Japan [project ID: jh250012 and jh260022], the Japan Society for the Promotion of Science (JSPS) KAKENHI [Grant No.: 24K07694], and the SECOM Science and Technology Foundation.

References

Chamberlain, M. A., Oke, P. R., Fiedler, R. A. S., Beggs, H. M., Brassington, G. B., and Divakaran, P.: Next generation of Bluelink ocean reanalysis with multiscale data assimilation: BRAN2020, Earth Syst. Sci. Data, 13, 5663–5688. https://doi.org/10.5194/essd-13-5663-2021, 2021.

Ciavatta, S., Brewin, R. J. W., Skákala, J., Polimene, L., de Mora, L., Artioli, Y., and Allen, J. I.: Assimilation of ocean-color plankton functional types to improve marine ecosystem simulations, JGR Oceans, 123, 834–854. https://doi.org/10.1002/2017JC013490, 2018.

Cossarini, G., Feudale, L., Teruzzi, A., Bolzon, G., Coidessa, G., Solidoro, C., Di Biagio, V., Amadio, C., Lazzari, P., Brosich, A., and Salon, S.: High-resolution reanalysis of the Mediterranean Sea biogeochemistry (1999–2019), Front. Mar. Sci., 8. https://doi.org/10.3389/fmars.2021.741486, 2021.

https://doi.org/10.5194/essd-2026-521
Preprint. Discussion started: 14 July 2026

Evensen, G.: The Ensemble Kalman Filter: Theoretical formulation and practical implementation, Ocean Dyn., 53, 343–367. https://doi.org/10.1007/s10236-003-0036-9, 2003.

Evensen, G.: Data assimilation: The Ensemble Kalman Filter, 2, Springer, Dordrecht, 307 pp. https://doi.org/10.1007/978-3-642-03711-5, 2009.

Fennel, K., Gehlen, M., Brasseur, P., Brown, C. W., Ciavatta, S., Cossarini, G., Crise, A., Edwards, C. A., Ford, D., Friedrichs, M. A. M., Gregoire, M., Jones, E., Kim, H.-C., Lamouroux, J., Murtugudde, R., Perruche, C., and the GODAE OceanView Marine Ecosystem Analysis and Prediction Task Team: Advancing Marine Biogeochemical and Ecosystem Reanalyses and Forecasts as Tools for Monitoring and Managing Ecosystem Health, Front. Mar. Sci., 6, 89, https://doi.org/10.3389/fmars.2019.00089, 2019.

Fisher, R. A. and Yates, F.: Statistical tables for biological, agricultural and medical research, Oliver & Boyd, London, 1948.

Ford, D. and Barciela, R.: Global marine biogeochemical reanalyses assimilating two different sets of merged ocean colour products, Remote Sens. Environ., 203, 40–54. https://doi.org/10.1016/j.rse.2017.03.040, 2017.

Gaspari, G. and Cohn, S. E.: Construction of correlation functions in two and three dimensions, Q. J. R. Meteorol. Soc., 125, 723–757. https://doi.org/10.1002/qj.49712555417, 1999.

Hafeez, M. A., Nakamura, Y., Suzuki, T., Inoue, T., Matsuzaki, Y., Wang, K., and Moiz, A.: Integration of Weather Research and Forecasting (WRF) model with regional coastal ecosystem model to simulate the hypoxic conditions, Sci. Total Environ., 771, 145290. https://doi.org/10.1016/j.scitotenv.2021.145290, 2021.

Hamill, T. M., Whitaker, J. S., and Snyder, C.: Distance-dependent filtering of background error covariance estimates in an ensemble Kalman Filter, Mon. Weather Rev., 129, 2776–2790. https://doi.org/10.1175/1520-0493(2001)129<2776:DDFOBE>2.0.CO;2, 2001.

Irie, M., Tsuji, Y., Nishida, S., Sakai, K., Nakashima, S., Nakahira, H., and Nakasuji, M.: Behavior of hypoxia in Osaka Bay; analysis of data collected at constant monitoring stations and visualization with water quality simulation, J. Jpn Soc. Civ. Eng. B2, 67, I_931–I_935. https://doi.org/10.2208/kaigan.67.I_931, 2011.

Matsuzaki, Y. and Inoue, T.: Perturbation of boundary conditions to create appropriate ensembles for regional data assimilation in coastal estuary modeling, JGR Oceans, 127. https://doi.org/10.1029/2021JC017911, 2022.

Matsuzaki, Y., Inoue, T., Kubota, M., Matsumoto, H., Sato, T., Sakamoto, H., and Naito, D.: Web application of an integrated simulation for aquatic environment assessment in coastal and estuarine areas, Environ. Modell. Softw., 181, 106184. https://doi.org/10.1016/j.envsoft.2024.106184, 2024.

Matsuzaki, Y., Inoue, T., Naito, D., and Mizuguchi, H.: Development of a physical analysis database for Ise Bay using regional coastal data assimilation, Japanese Journal of JSCE, 81, n/a. https://doi.org/10.2208/jscejj.25-17173, 2025a.

Matsuzaki, Y. and Kubota, M.: Uncertainty in river discharge forcings and error range on nowcasting numerical simulation of salinity and seawater temperature in Ise Bay, Japan, Mar. Pollut. Bull., 207, 116734. https://doi.org/10.1016/j.marpolbul.2024.116734, 2024.

Matsuzaki, Y., Kubota, M., Inoue, T., and Mizuguchi, H.: Ecological hydrodynamic modeling and factor analysis of hypoxia dissipation in the semi-enclosed Mikawa Bay, Japan, in August 2020, Mar. Pollut. Bull., 218, 118190. https://doi.org/10.1016/j.marpolbul.2025.118190, 2025b.

https://doi.org/10.5194/essd-2026-521
Preprint. Discussion started: 14 July 2026

Matsuzaki, Y., Mizuguchi, H., and Inoue, T., Ise Bay ReAnalysis (IBRA): A Subset Ecological Hydrodynamic Dataset Based on EcoPARI (2011–2022), [Data set]. Zenodo. https://doi.org/10.5281/zenodo.19808667

Mizuguchi, H., Matsuzaki, Y. and Inoue, T.,: A study on improvement of reproducibility of bottom-water intrusion from open ocean into mikawa bay in August 2020, using a regional coastal data assimilation, Japanese Journal of JSCE, 81, 17, http://10.2208/jscejj.25-17102, 2025

Munk, W. H. and Anderson, E. R.: Notes on a theory of the thermocline, J. Mar. Res., 7, 1948.

Nagano, T.: ata assimilation of dissolved oxygen in Osaka Bay using a 4D-Var framework: 128 pp, Ph.D. thesis, Osaka University, Japan (in Japanese), University of Osaka, Osaka, 2025. https://doi.org/https://doi.org/10.18910/103228.

Orlanski, I.: A simple boundary condition for unbounded hyperbolic flows, J. Comput. Phys., 21, 251–269. https://doi.org/10.1016/0021-9991(76)90023-1, 1976.

Sanikommu, S., Toye, H., Zhan, P., Langodan, S., Krokos, G., Knio, O., and Hoteit, I.: Impact of atmospheric and model physics perturbations on a high-resolution ensemble data assimilation system of the Red Sea, JGR Oceans, 125. https://doi.org/10.1029/2019JC015611, 2020.

Sekine, Yoshihiko, Shogo Nakamura, and Ya Wei Wang. 2002. “Variation in Wind in the Region around Ise Bay.” The Bulletin of the Faculty of Bioresources. Mie University 28: 1–9.

Smagorinsky, J.: General circulation experiments with the primitive equations: I. The basic experiment, Mon. Weather Rev., 91, 99–164. https://doi.org/10.1175/1520-0493(1963)091<0099:GCEWTP>2.3.CO;2, 1963.

Tanaka, Y., Nakamura, Y., Suzuki, K., Inoue, T., and Nishimura, Y.: Development on the pelagic ecosystem model considering the microbial loop for estuary and coastal areas, report of the port and airport Research Institute, 50, 3–68, 2011.

Tanaka, Y. and Suzuki, K.: Development of non-hydrostatic numerical model for stratified flow and upwelling in estuary and coastal areas, report of the port and airport Research Institute, 49, 3–26, 2010.

Von Schuckmann, K., Le Traon, P.-Y., Smith, N., Pascual, A., Brasseur, P., Fennel, K., Djavidnia, S., Aaboe, S., Fanjul, E. A., Autret, E., Axell, L., Aznar, R., Benincasa, M., Bentamy, A., Boberg, F., Bourdallé-Badie, R., Nardelli, B. B., Brando, V. E., Bricaud, C., Breivik, L.-A., Brewin, R. J. W., Capet, A., Ceschin, A., Ciliberti, S., Cossarini, G., De Alfonso, M., De Pascual Collar, A., De Kloe, J., Deshayes, J., Desportes, C., Drévillon, M., Drillet, Y., Droghei, R., Dubois, C., Embury, O., Etienne, H., Fratianni, C., Lafuente, J. G., Sotillo, M. G., Garric, G., Gasparin, F., Gerin, R., Good, S., Gourrion, J., Grégoire, M., Greiner, E., Guinehut, S., Gutknecht, E., Hernandez, F., Hernandez, O., Høyer, J., Jackson, L., Jandt, S., Josey, S., Juza, M., Kennedy, J., Kokkini, Z., Korres, G., Kõuts, M., Lagemaa, P., Lavergne, T., Le Cann, B., Legeais, J.-F., Lemieux-Dudon, B., Levier, B., Lien, V., Maljutenko, I., Manzano, F., Marcos, M., Marinova, V., Masina, S., Mauri, E., Mayer, M., Melet, A., Mélin, F., Meyssignac, B., Monier, M., Müller, M., Mulet, S., Naranjo, C., Notarstefano, G., Paulmier, A., Gomez, B. P., Gonzalez, I. P., Peneva, E., Perruche, C., Andrew Peterson, K., Pinardi, N., Pisano, A., Pardo, S., Poulain, P.-M., Raj, R. P., Raudsepp, U., Ravdas, M., Reid, R., Rio, M.-H., Salon, S., Samuelsen, A., Sammartino, M., Sammartino, S., Sandø, A. B., Santoleri, R., Sathyendranath, S., She, J., Simoncelli, S., Solidoro, C., Stoffelen, A., Storto, A., Szerkely, T., Tamm, S., Tietsche, S., Tinker, J., Tintore, J., Trindade, A., van Zanten, D., Vandenbulcke, L., Verhoef, A., Verbrugge, N., Viktorsson, L., von Schuckmann, K., Wakelin, S. L., Zacharioudaki, A., Zuo, H.: Copernicus marine service ocean state report, J. Oper. Oceanogr., 11 (sup1), S1–S142. https://doi.org/10.1080/1755876X.2018.1489208, 2018.

Westrich, J. T. and Berner, R. A.: The role of sedimentary organic matter in bacterial sulfate reduction: The G model tested1, Limnol. Oceanogr., 29, 236–249. https://doi.org/10.4319/lo.1984.29.2.0236, 1984.

https://doi.org/10.5194/essd-2026-521
Preprint. Discussion started: 14 July 2026

Wilkin, J., Levin, J., Moore, A., Arango, H., López, A., and Hunter, E.: A data-assimilative model reanalysis of the U. S. Mid Atlantic Bight and Gulf of Maine: Configuration and comparison to observations and global ocean models, Prog. Oceanogr., 209, 102919. https://doi.org/10.1016/j.pocean.2022.102919, 2022